To the Graduate Council:

I am submitting herewith a thesis written by Jason Michael Cunningham entitled "Characterization of High-Temperature Superconductor Film Layers Using Raman Spectroscopy." I have examined the final copy of this thesis for form and content and recommend that it be accepted in partial fulfillment of the requirement for the degree of Master of Science, with a major in Physics.

Horace Crater

Horace Crater, Major Professor

We have read this thesis
and recommend its acceptance

Accepted for the Council:

Associate Vice Chancellor and
Dean of The Graduate School

Characterization of High-Temperature Superconductor Film Layers Using Raman Spectroscopy

A Thesis

Presented for the

Master of Science

Degree

The University of Tennessee, Knoxville

Jason Michael Cunningham

December, 1998

Thesis
98
.C86

Acknowledgments

There are several people I would like to thank for their assistance and patience during my time at the University of Tennessee Space Institute. I would like to thank my Thesis Committee, Dr. Horace Crater, Dr. Jim Lewis, and Dr. Christian Parigger, for their efforts in helping me to finish this thesis. They have read my previous versions of this thesis and this final draft is due in large part to their suggestions and contributions.

I would also like to thank my research supervisor, Dr. Brad Winkleman. He helped me through some very trying times in the laboratory and tried to make sure that I had as many working parts at one time as possible.

I also need to thank the authors who have allowed me to reproduce figures from their papers. I would like to thank Drs. Jahanzeb, Celik-Butler, Shan, and Butler for allowing me to use their paper from Journal of Applied Physics, December 1, 1995 [21]. Also, I need to thank Drs. Zhang, Haage, Habermeier, Ruf, and Cardona for allowing me to use their paper from Journal of Applied Physics, September 1, 1996 [23].

Lastly, I would like to thank my wife, Heather. She reviewed the earlier versions of this thesis and helped to correct my own poor grammar skills.

Abstract

High-temperature superconductor films can be characterized using Raman spectroscopy to obtain the crystal orientation, oxygen concentration, and layer thickness for the film layers. This information is essential in determining characteristics of the films, such as transition temperature and current density. Good quality films need high transition temperature and current density.

Previously published work shows that the theory and background work on Raman spectroscopy on high-temperature superconductor films gives this information. Earlier research on high-temperature superconductor films shows how the films can be characterized. By applying these different methods Raman data can be used as an effective analytical technique.

An experimental setup is designed to evaluate the feasibility of acquiring the data quickly in an industrial environment using alternate technology than that used by previous reseachers. Previous work in this area has been constricted to microprobe techniques which study single crystals of the superconductor. A technique is used which could give overall Raman data from a large area of the film, as opposed to single crystals or grains.

Background and experimental work described in this thesis describes a method for determining layer thickness in buffer and superconducting film layers. Data is collected from a single film sample and a proposed buffer layer sample. This data is used to identify necessary improvements to the basic experimental setup to create a real-time, in situ, Raman diagnostic setup for use in industrial, high-temperature superconductor film processes.

Table of Contents

Chapter Page

I. Introduction 1

II. Theoretical Background 4

A. Raman scattering from crystals 4

B. Description of YBCO Raman lines 6

III. Survey of Experimental Research Methods 10

A. Oxygen content 10

B. Crystal orientation 11

C. Layer thickness 15

D. Diamond and silicon films 20

IV. Investigation of Raman Spectroscopy Experimental Setup 22

A. Design 22

B. Testing electronics 24

C. Calibration procedures 24

D. Data from calibration samples 28

E. YBCO film sample 29

F. $LaAlO_3$ sample 36

V. Improvements to Experimental Setup for Industrial Applications 39

VI. Conclusion 44

References 46

Vita 50

List of Figures

Figure		Page
2.1	Crystalline Structure of YBCO	7
3.1	Raman spectra for two samples on side of film(solid) and middle of film (dashed) [21]	14
3.2	Raman spectra of YBCO films with different thicknesses as-recorded [23]	16
3.3	Raman spectra of YBCO films after subtraction of substrate [23]	17
3.4	Difference in Raman Lines vs. YBCO Layer Thickness	19
3.5	Ratio of Raman Lines vs. YBCO Layer Thickness	19
4.1	Raman Spectroscopy Experimental Setup	23
4.2	Photon Counts vs. Integration Time	26
4.3	Log of Photon Counts vs. Log of Integration Time	26
4.4	Standard Deviation/Counts vs. Integration Time	27
4.5	Log of Standard Deviation/Counts vs. Integration Time	27
4.6	Raman Scan on Diamond Sample	28
4.7	Raman Scan of Sulphur Powder	30
4.8	Raman Scan of YBCO Film (yy-polarization)	31
4.9	Raman Scan of YBCO Film (xyxy-polarization)	32
4.10	Raman Scan of YBCO Film (xx-polarization)	32
4.11	Raman Scan of YBCO Film (yx-polarization)	33
4.12	Raman Scan of YBCO Film (yxxy-polarization)	33

4.13 Raman Scan of YBCO Film (xy-polarization) 34

4.14 Raman Scan on YBCO 35

4.15 Raman Scan on YBCO Near 335 line 35

4.16 Raman Scan on Lanthanum Aluminate Layer 37

4.17 Raman Scan on Lanthanum Aluminate Film Substrate 37

4.18 Raman Scan on Thin Layer of Lanthanum Aluminate 38

List of Tables

Table		Page
2.1	Experimental Raman bands for YBCO	8

I. Introduction

The scientific applications of superconductivity in commerce and industry have been broadened by the discovery of ceramic superconductors, or high-temperature superconductors (HTSC) [1]. Since the discovery of high-temperature superconductivity in 1987 research has expanded in an effort to find higher temperature superconductors and create techniques to process HTSC materials into practical forms such as wire, ribbon, and films that retain the properties of HTSC. Creating HTSC films with high current densities ($\sim 10^6$ A/cm^2) in long kilometer lengths has become the major goal to be achieved for industrial and commercial applications [2].

The creation of HTSC films with high current densities has been achieved in laboratories with smaller lengths of films, but has not as yet been achieved for longer lengths of film [2]. Some of the techniques used include metal-organic chemical vapor deposition (MOCVD), pulsed laser deposition (PLD), sol-gel, metal-organic deposition (MOD), chemical vapor deposition (CVD), electrophoresis, electrodeposition, ion beam assisted deposition (IBAD), and aerosol/spray pyrolysis.

Forms of each of these processes have been designed to create longer lengths of HTSC films. These proposed industrial designs have been studied for diagnostic and parameter controls. Parameters such as temperature, pressure, or layer thickness must be monitored during the application process to ensure the films are of high quality. Decisions were made about what parameters would need to be measured at any point in each of the processes. Then, information was gathered concerning each measurement, such as the range of the measurement, the accuracy needed in measuring it, the technology to be used to make the measurement, the cost of the technology, and any comments about the

process. Little of this information is available in the current literature since research in this area is still proceeding and none of the specific techniques have been universally accepted as the preferred technique. The data collected from this research is printed in a DOE Topical Report presented by UTSI [3].

After a thorough study of each of these techniques, the need for system control of HTSC layer deposition has been established. Only films of high quality will be useful in industrial and commercial applications, therefore the film quality must be monitored to insure that films with high current density and high transition temperature are being manufactured [2].

Several of the parameters of the films that must be monitored are crystal orientation, oxygen concentration, morphology, grain size, and layer thickness. Of these parameters crystal orientation, oxygen concentration, and layer thickness play major roles in determining the current density and transition temperature of the films [2, 4, 5, 6, 7].

Current flow in a HTSC film is directly related to the crystal orientation and layer thickness of the films. The better aligned the axes of the crystal for the appropriate layer thickness the higher the current density in the film. Also, the transition temperature is directly related to the oxygen concentration of the crystal. The higher the oxygen concentration the higher the transition temperature will be.

Techniques must be developed to monitor these three important characteristics of the HTSC. The technique discussed in this thesis is Raman spectroscopy. "Raman spectroscopy in the 1990s is one of the most versatile methods for chemical measurements of molecular species. It can be used for routine qualitative and quantitative measurements of both inorganic and organic materials, and it is successfully employed to solve complex

analytical problems such as determining chemical structures." [8] "Raman spectroscopy is a powerful analytical investigation technique for studying phonons in solid with relatively simple instrumentation." [9]

The volume of information that Raman spectroscopy provides as well as its versatility makes it a viable and very valuable technique especially in the field of HTSC diagnostics. Raman spectroscopy can be used as a tool for acquiring information on crystal orientation, layer thickness, and oxygen concentration of HTSC films in situ.

In this thesis a rudimentary introduction to the theory of Raman scattering from HTSCs will be presented. Then, the background material necessary for understanding prior Raman work on $YBa_2Cu_3O_{7-x}$ (YBCO), the type of HTSC studied in this thesis, will be presented. How Raman spectroscopy can determine the parameters of a YBCO film will be described. The Raman spectroscopy experimental setup used for collecting data in this thesis is explained in the following section. Data collected on a YBCO film sample and a buffer layer sample are presented in the next section. In the following section, improvements necessary to adapt the Raman experimental setup to industrial applications are discussed. The final chapter of this thesis presents possibilities for future work in this area.

II. Theoretical Background

Raman scattering theory will not be treated rigorously here because there are several references which give a thorough description of the subject [9, 10, 11]. A general outline of the theory of Raman scattering from a solid and specifically from a HTSC will be presented here.

A. Raman scattering from crystals

The following is based upon the theoretical presentation by Neil W. Ashcroft and N. David Mermin in the book Solid State Physics [12]. The interaction of a wave with lattice vibrations of a crystal will be examined.

First, the incident wave has angular frequency $\frac{E}{\hbar}$ and wave vector $\vec{q} = \frac{\vec{p}}{\hbar}$. This wave interacts with a normal mode of the crystal with angular frequency ω and wave vector $\vec{k}$. Only this particular normal mode is excited and is regarded as a wavelike disturbance in a continuous medium. The scattering wave has wave vector $\vec{q}'$. The disturbance is moving with the phase velocity

$$\vec{v} = \frac{\omega}{k}\vec{k}. \tag{1}$$

Bragg reflection will be used to describe this process. The Bragg condition can be written as

$$m\lambda = 2d\sin\theta \tag{2}$$

where m is an integer giving the order of the reflection, d is the distance between two lattice planes where $d = \frac{2\pi}{k}$, and the wave vector $\vec{q}$ makes an angle θ with the lattice. Therefore, equation (2) can be written as

$$\frac{2\pi m}{q} = \frac{4\pi}{k}\sin\theta \tag{3}$$

or

$$mk = 2q\sin\theta \tag{4}$$

or

$$mk = (\vec{q}'-\vec{q})\cdot\hat{k} \tag{5}$$

Because the angle of incidence equals the angle of reflection and the magnitude of q' equals the magnitude of q, it follows that $\vec{q}'-\vec{q}$ must be parallel to $\vec{k}$, then

$$\vec{q}'-\vec{q} = m\vec{k} \tag{6}$$

The diffraction is described in the frame of reference that moves with the phase velocity $\vec{v}$ where the disturbance is stationary, and the Bragg condition can be applied. The wave vectors of the lattice, incident, and scattered waves are unaltered by a change of reference frame, because neither the distance between planes of constant phase nor their orientation is affected. The frequencies undergo a Doppler shift :

$$\overline{\omega} = \omega - \vec{k}\cdot\vec{v} \tag{7}$$

$$\frac{\overline{E}}{\hbar} = \frac{E}{\hbar} - \vec{q}\cdot\vec{v} \tag{8}$$

$$\frac{\overline{E}'}{\hbar} = \frac{E'}{\hbar} - \vec{q}'\cdot\vec{v} \tag{9}$$

$\overline{E}'$ must equal $\overline{E}$ since Bragg reflection by a stationary grating does not alter the frequency of the incident wave. Therefore equation (8) equals equation (9) to show that in the original frame the frequency of the scattered wave must be shifted:

$$\frac{E'}{\hbar} = \frac{E}{\hbar} + (\vec{q}' - \vec{q}) \cdot \vec{v}. \tag{10}$$

The change in wave vector under a Bragg reflection has the form:

$$\vec{q}' = \vec{q} + m\vec{k} \tag{11}$$

where m is the order of the Bragg reflection. This relation holds in either frame of reference, since wave vectors are invariant under change of frame of reference.

By substituting equation (11) into equation (10) the frequency shift in the original frame of reference is found to be :

$$E' = E + m\hbar\omega\,. \tag{12}$$

Notice here that m can be positive or negative corresponding to Stokes or anti-Stokes Raman scattering. Processes involving several modes will correspond to successive Bragg reflections from the corresponding moving diffraction gratings. This can also be seen as an mth-order Bragg reflection in the moving frame corresponding to a process that would be described in the laboratory frame as the absorption or emission of m phonons.

The Raman shift is measured in wavenumbers or cm^{-1}. This is the typical nomenclature used in Raman spectroscopy. The notation, cm^-1, is also used in this thesis to denote a Raman shift in wavenumbers.

B. Description of YBCO Raman lines

YBCO consists of 13 atoms and has an orthorhombic or tetragonal unit cell with a = 3.818, b = 3.889, and c = 11.68 Angstroms and belongs to the D_{2h} point group and Pmmm space group [13]. Figure 2.1 shows a unit cell of YBCO. It has two dimpled plane layers Cu(2)-O(2)-O(3) that form a two-dimensional rectangular network and a linear

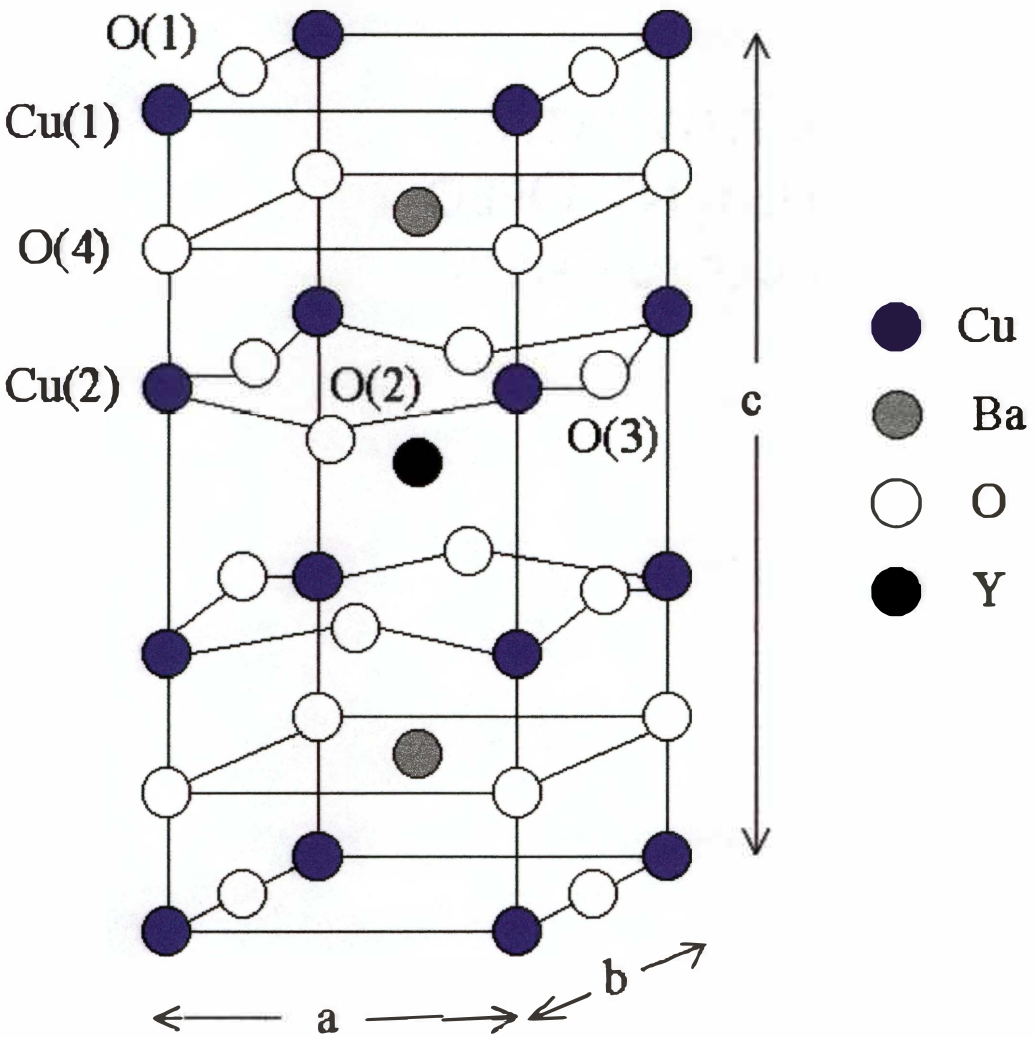


Figure 2.1 Crystalline Structure of YBCO

chain Cu(1)-O(1) [13]. The O(4) oxygen atom forms a bridge between the Cu(1) and Cu(2) copper atoms.

There are three different types of Raman modes for YBCO. One mode that corresponds to axial motion along the c axis is known as the A_g mode. Two other modes, known as B_{2g} and B_{3g} modes, represent transverse motions along the a and b axes and are about 100 times weaker than the A_g mode. Another mode that appears in YBCO, a B_{1g} mode, is a pseudotetraganol mode. Table 2.1 shows some Raman lines for YBCO and the assignment for each.

Frequency (cm^{-1})	Symmetry	Atom mainly involved
108	A_g	Ba, axial
120-140	A_g	Ba, axial
154	A_g	Cu(2) in CuO_2 plane, axial
335	B_{1g}	O(2,3) out-of-phase, axial
435	A_g	O(2,3) in-phase, axial
500	A_g	O(4) bridge, axial

Table 2.1 Experimental Raman bands for YBCO

The vibrations of the oxygen atoms lie in the 300 cm^{-1} - 700 cm^{-1} ranges, therefore each Raman line corresponds to a motion of a particular oxygen atom occupying a definite site because little intermixing exists between the vibrations of the different atoms. "The Raman technique is thus a selective probe of each oxygen site." [10]

Four Raman lines to be studied in this thesis are the lines at 335, 435, 500, and 640 cm^{-1}. The Raman line at 500 cm^{-1} is due to axial symmetric vibrations of the O(4) oxygen atom between the two coppers. It is an A_g mode and has a cc-polarization, which refers

to incident radiation polarized along the c-axis of the crystal and scattered radiation polarized along the c-axis. The 435 cm^{-1} line is also an A_g mode. It is assigned to O(2), O(3) in phase binding motion, consistent with cc-polarization. The 335 cm^{-1} line is a B_{1g} mode and corresponds to O(2), O(3) out of phase binding motion. It is present in aa-polarizations. A line that appears at 640 cm^{-1} is caused by a $BaCuO_2$ impurity phase. This just appears in ceramics, not in single crystals of YBCO [20].

III. Survey of Experimental Research Methods

Previous work on Raman spectroscopy of high-temperature superconductors, especially with YBCO, has provided important information about the HTSC. Detailed descriptions of the Raman scattering of HTSC have been published by Thomsen and Cardona, Kuzmany et al., Feile, Ferraro and Maroni, and Eric Faulques and Richard Russo [8].

The very first investigation of $YBa_2Cu_3O_{7-x}$ single crystals was made by Hemley and Mao on microcrystals using micro-Raman spectroscopy [15]. They found three of the A_g modes. New results found by McCarty et al and other groups were successful in determining the other Raman modes [14, 16].

These studies into the lattice dynamics of the high-temperature superconductors were a great source of data on the structural features and the nature of the interatomic interactions [17]. This information was important for reaching an understanding of the mechanism of the superconducting transition. The physical properties of $YBa_2Cu_3O_{7-x}$ are known to depend strongly on the oxygen content, crystal orientation, and layer thickness.

A. Oxygen content

An important feature of YBCO films is the oxygen content. The structure and thus the transition temperature of $YBa_2Cu_3O_{7-x}$ is dependent on x, the oxygen content of the crystal. The x in the subscript of the oxygen in YBCO can vary from 1 to 0. Decimal values for x refer to an average over many YBCO crystals. YBCO has two forms, the superconducting crystal which has an orthorhombic structure and the semiconducting crystal which has a tetragonal structure. The transition from one state to another takes place for x approximately equal to .5. As x decreases from .5 to 0 the transition

temperature of the crystal increases. YBCO has a transition temperature of 94 K for x = 0 and a transition temperature of about 55 K for x = .5 [7, 18].

The Raman line at 500 cm^{-1} corresponds to the stretching of the O(4) oxygen atom and thus corresponds to the oxygen concentration of the crystal. The Raman line lies about 502 cm^{-1} for x = 0 and shifts to a lower wavenumber as x increases [7]. By studying the placement of this Raman line, an accurate number for the transition temperature of the crystal can be determined.

B. Crystal orientation

The crystal orientation of YBCO is another important aspect of the structure of YBCO. Crystal orientation has a direct relationship to the current density. Crystals with a higher degree of axes alignment have a higher current density [2, 20].

The crystal orientation for a YBCO film can also be determined by studying the Raman spectra of the film. To get an overall idea of the crystal orientation of a piece of HTSC film, Raman spectra must be taken on different places of the film using different polarizations and orientations.

First, the degree of c-axis tilt can be found by studying two specific Raman lines. In "Influence of the growth rate of $YBa_2Cu_3O_{7-\delta}$ films on the orientation of the crystallographic axes" the authors, S.F. Karmanenko et al [20], found that the ratio of the 500 cm^{-1} and the 335 cm^{-1} lines will give the degree of c-axis tilt. They studied films with c-axis perpendicular to the surface, or (001)-oriented, and c-axis parallel to the surface of the film, or (100)-oriented. They determined that the fraction of (100)-oriented crystallites is given by

$$Z \approx \frac{(2.5q - 1)}{(12.5 + q)} \tag{13}$$

where q is given by

$$q = \frac{I_{500}}{I_{335}} \tag{14}$$

I_{500} and I_{335} are the intensities of the line at 500 cm^{-1} and the line at 335 cm^{-1}, respectively.

Karmanenko et al also determined that in films consisting of a mixture of the two orientations that q varies from 0.4 for a (001) film orientation to 9 for a (100) film orientation. An estimate of the fraction of crystallites aligned in a certain direction can be determined by using equation (13).

From these not only can the degree of c-axis tilt for a particular crystal be found, but an overall degree of homogeneity in the area of the excited crystal can also be determined. Equation (13) gives the percentage of (100)-oriented crystallites and thus an idea of the overall c-axis orientation.

High quality films must have a (001)-orientation. In such films the current flows in the corrugated copper-oxygen planes. This allows for a high current density. The more crystallites with high degree of c-axis alignment the higher the current density will be for the film.

The entire film must be studied to insure that it has a uniform crystal orientation throught. A. Jahanzeb, et al in "Studies and implications of the Hall effect in superconducting and semiconducting $YBa_2Cu_3O_{7-\delta}$ thin films" studied two different films, one that is homogeneously oriented and another with a mixture of different orientations

[21]. In Fig. 3.1 taken from this paper, the change in the spectra when different parts of the film are scanned. The solid lines are spectra taken from the side of the film and the dotted lines are spectra taken from the middle of the film. Notice that the spectrum for film A does not change as the length of the film is scanned while the spectrum for film B does change. This suggests that film A has homogeneous orientation and film B can be a mixture of different orientations.

The appearance of the 500 and 640 cm^{-1} lines are due to the lack of c-axis orientation. The 640 line is from the $BaCuO_2$ phase that can sometimes exist at the boundaries of $YBa_2Cu_3O_{7-\delta}$ grains. Therefore, film B has mixed orientations.

The overall crystal orientation can be found by studying the different polarizations. M.V. Belousov et al. studied six different films with different orientations of the crystallographic axes in "Raman scattering of light used as a method of analyzing the oriented $YBa_2Cu_3O_{7-\delta}$ films" [22]. To describe the scattering geometry the authors used the laboratory coordinate system x,y,z. The a, b, and c crystallographic axes are shown in Fig. 2.1 . The authors studied several different films.

Films showing strong (100)-orientation as seen from the xx polarization were rotated 90^{O} about the axis perpendicular to the surface of the film. As a result the spectra retained only weak lines at 500 cm^{-1} and 580 cm^{-1}. These spectra also didnt have a line at 335 cm^{-1} so the a-axis in one film and the b-axis in the other film lie at a 45^{O} angle with respect to the surface.

Another film exhibited strong lines at 500, 410, and 335 cm^{-1} in the xx-

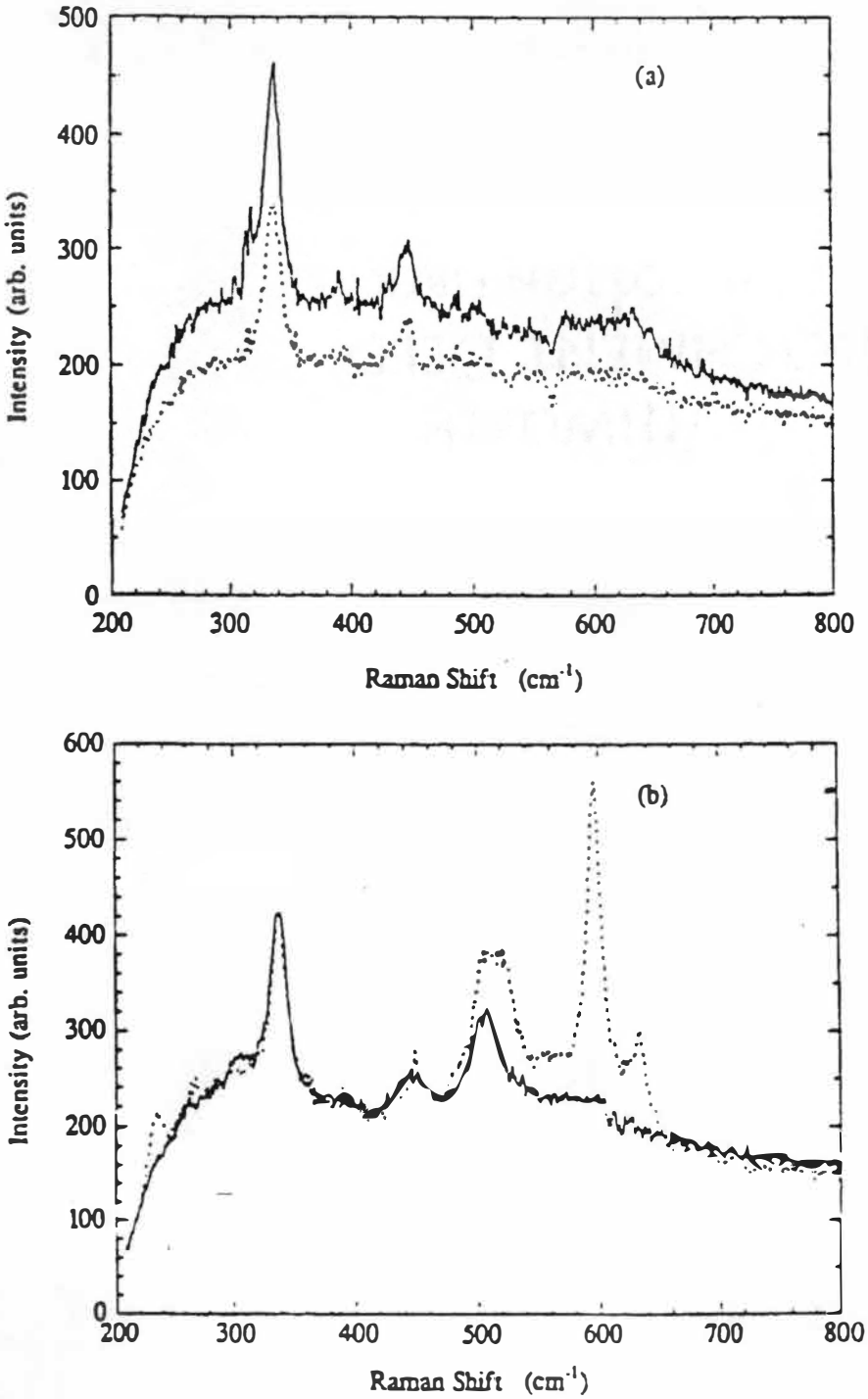


Fig. 3.1 Raman spectra for two samples on side of film (solid) and middle of film (dashed)
Source: Jahanzeb, Al, et. al., Journal of Applied Physics, Vol. 78, December 1, 1995. Reprinted by permission of the American Institute of Physics.

polarization. The authors noticed the intensity of the Raman scattering in the xz polarization was minimal when the crystallographic axes of the substrate were parallel to x. This film consisted of microscopic regions with mutually perpendicular positions of the axes, b perpendicular to the normal and c perpendicular to the normal.

Another film had spectrum similar to that of light from the ab plane of a bulk single crystal. As the polarization went to ab the intensity of the Raman scattering decreased indicating a high degree of orientation of the film.

The intensity of the Raman scattering in another film did not depend on orientation. The ratio of the intensities of the 500 cm^{-1} and the 332 cm^{-1} lines suggested the c-axis was at an angle to the surface.

The authors of this paper used several techniques to determine the crystal orientation of each film. They used the technique described earlier to determine the degree of c-axis tilt and observed spectra in different polarizations to determine the overall crystal orientation. Information on the orientation of the a- and b-axes was also obtained.

C. Layer thickness

Another important feature of any layer in a HTSC film is layer thickness. Specifically in the YBCO layer the layer thickness is related to the current density [1]. Thus measurements of layer thickness along with crystal orientation could give a measurement for the current density, so as to insure that high quality films are being formed.

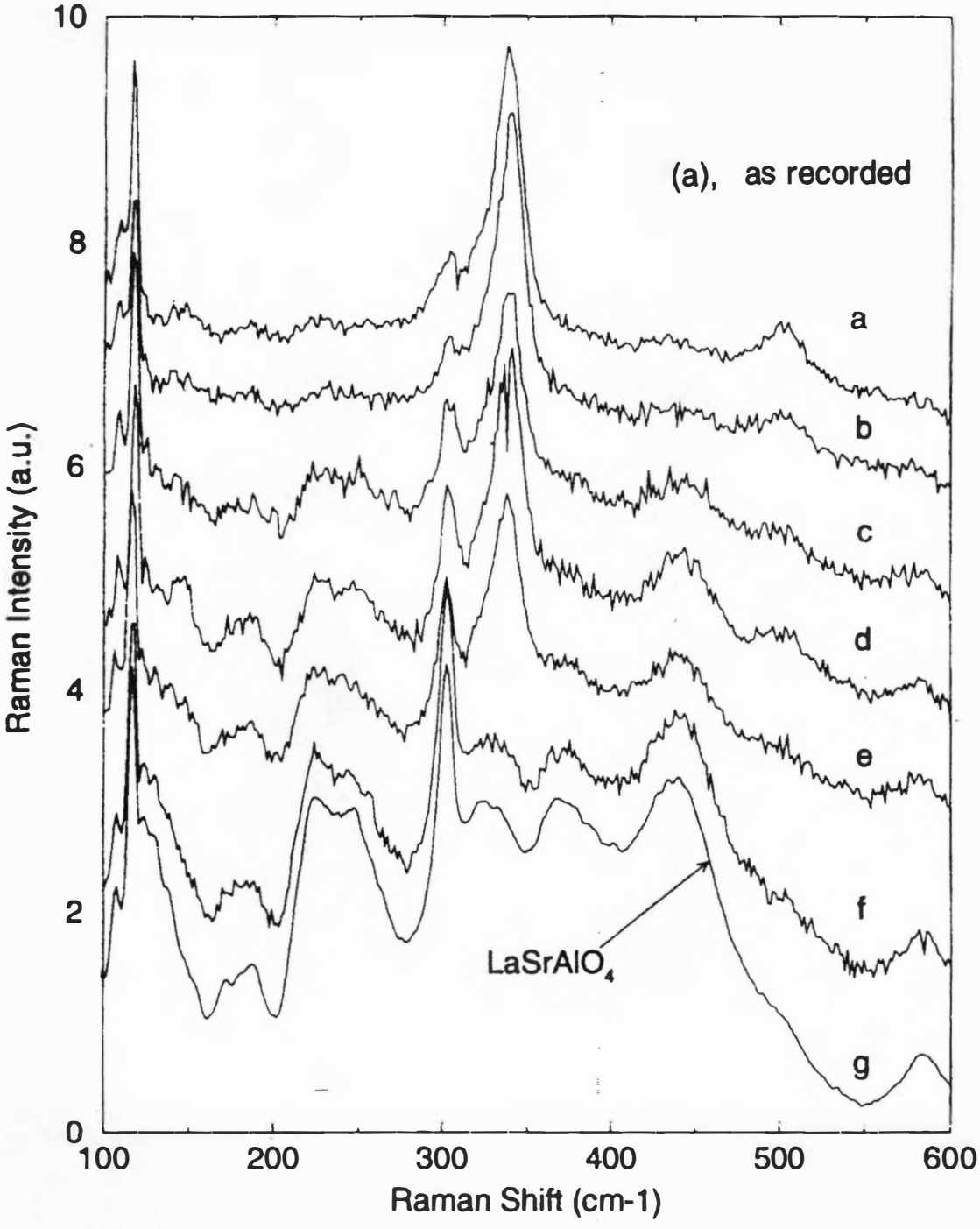


Fig. 3.2 Raman spectra of YBCO films with different thicknesses as-recorded
Source: Zhang, P., et. al., Journal of Applied Physics, Vol. 80, Sep. 1, 1996.
Reprinted by permission of the American Institute of Physics.

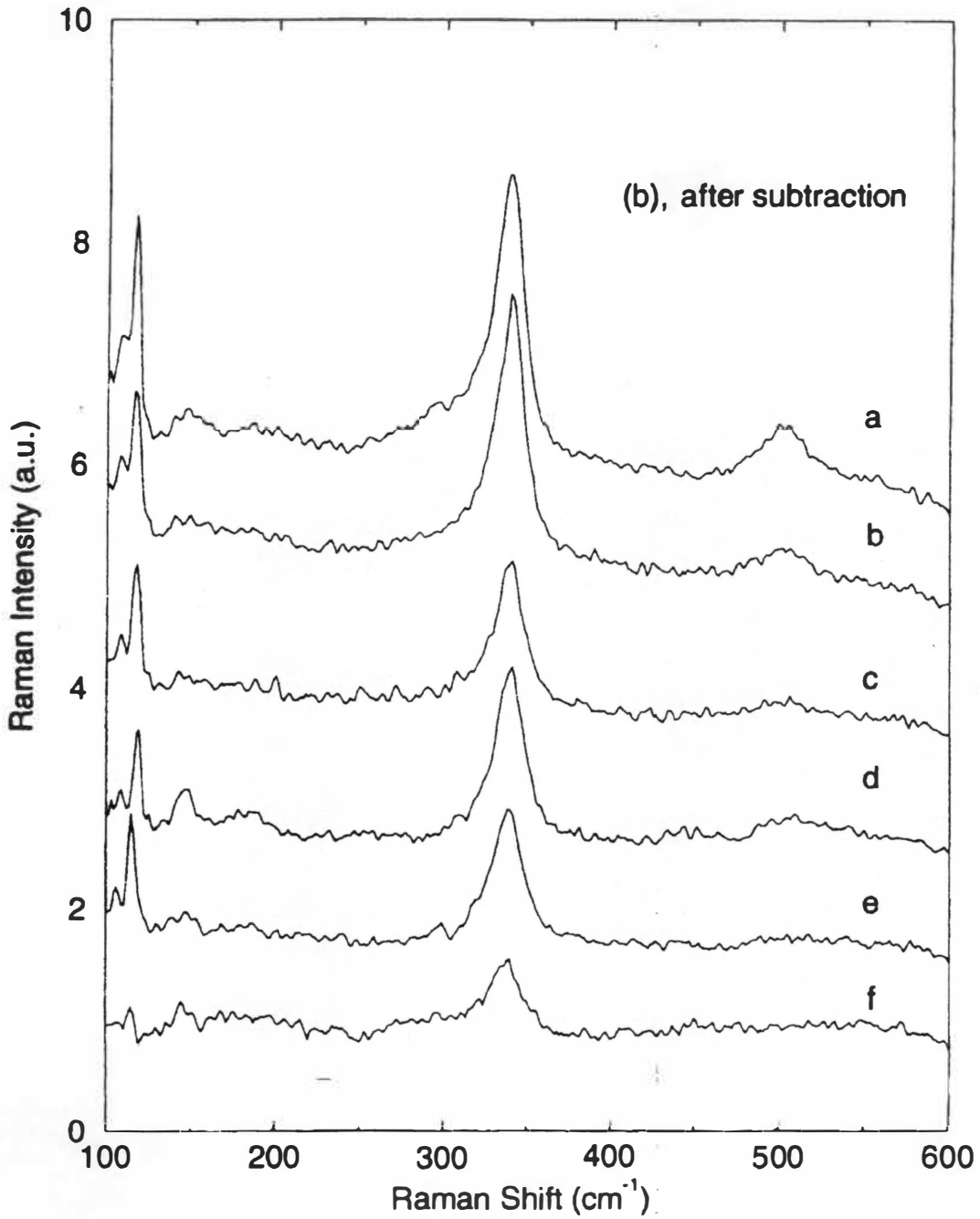


Fig. 3.3 Raman spectra of YBCO films after subtraction of substrate
Source: Zhang, P. et. al., Journal of Applied Physics, Vol. 80, Sep. 1, 1996.
Reprinted by permission of the American Institute of Physics.

In "Raman spectra of ultrathin $YBa_2Cu_3O_{7-\delta}$ films" P. Zhang et al [23] studied Raman spectra from different films with different layer thickness. Figures 3.2 and 3.3 are taken from this paper.

The thicknesses for the films are (a) 240, (b) 120, (c) 60, (d) 36, (e) 24, and (f) 12 nm where Fig. 3.2 shows the as-recorded spectra and Fig. 3.3 shows the spectra after subtraction of the substrate features.

The plot in Fig. 3.2 was used to obtain data presented in Figs. 3.4 and 3.5. The Raman intensities for the 335 cm^{-1} from the YBCO layer and the 300 and 225 cm^{-1} lines from the substrate were taken from Fig. 3.2. Figure 3.4 shows the difference in the Raman lines, substrate Raman lines subtracted from the YBCO Raman line, plotted versus the YBCO layer thickness. Figure 3.5 shows the ratio of the Raman lines, substrate Raman lines divided by the YBCO Raman line, plotted versus the YBCO layer thickness. Though no Raman peak is visible for spectra taken from no YBCO layer and 12 nm YBCO layer thickness the intensity was taken at the 335 Raman shift.

Each plot seems to show a general trend with the exception of the points at 60 nm of YBCO layer thickness. Reasons for this could be that the data taken from this film sample is inaccurate at this layer thickness, or that the film goes through a transition at this layer thickness. More research must be done to determine what the reason is for this deviation.

These figures do show that there is a relationship between the Raman lines taken from the two layers and YBCO layer thickness. Thickness of a YBCO layer could be determined by measuring the Raman line intensities from the two different layers and

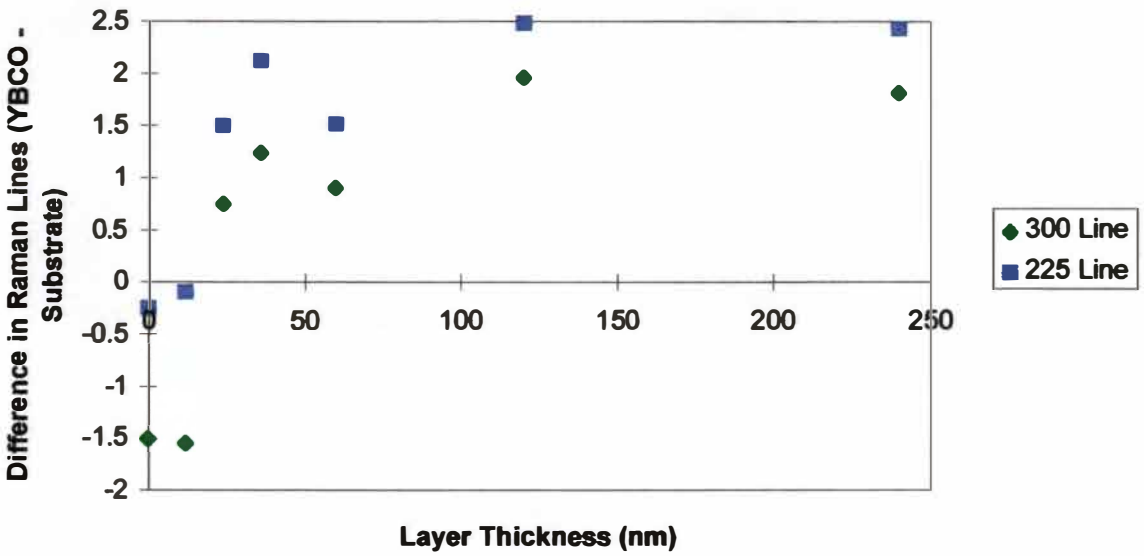


Fig. 3.4 Difference in Raman Lines vs. YBCO Layer Thickness
Source: Zhang, P., et. al., Journal of Applied Physics, Vol. 80, Sep. 1, 1996.

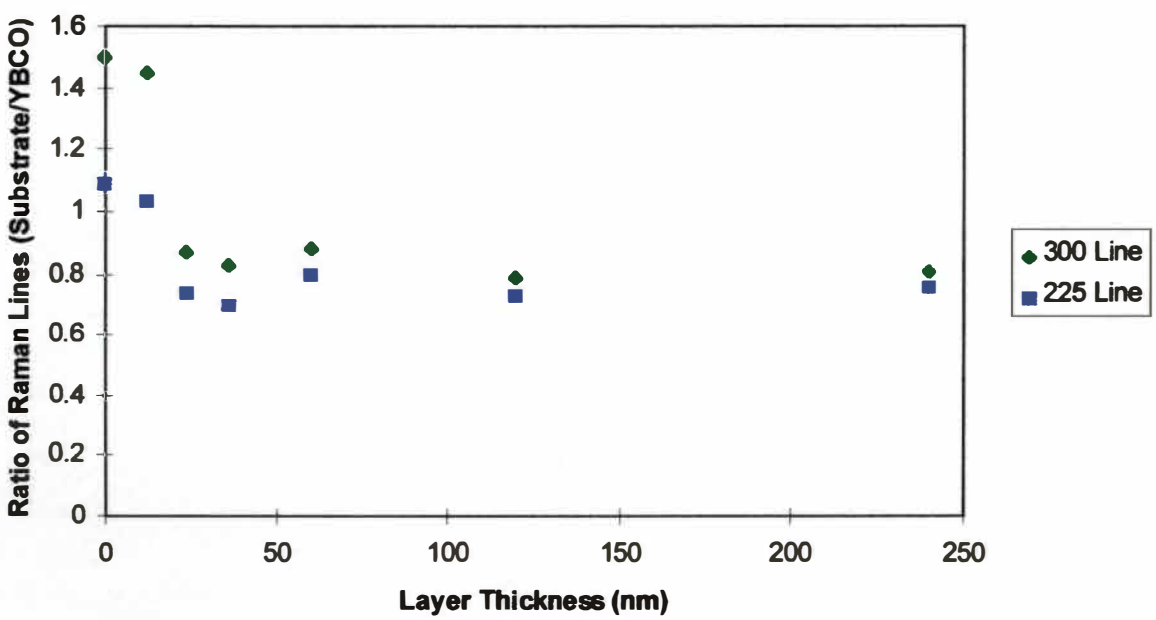


Fig. 3.5 Ratio of Raman Lines vs. YBCO Layer Thickness
Source: Zhang, P., et. al. Journal of Applied Physics, Vol. 80, Sep. 1, 1996.

fitting this measurement to figures similar to Figs. 3.4 and 3.5. These measurements could be limited by the nature of the figures. This technique might only be applicable to thicknesses from about 20 nm to 100 nm. For thicknesses not in this range the trend in the figures approaches a line making this technique less accurate.

D. Diamond and Silicon Films

Another technique, yet to be studied using YBCO films, has been used on diamond and silicon films [24, 25, 26, 27, 28]. This technique studies the intensity of a Raman line as either or both of the incident polarization vector and the scattered polarization vector are rotated.

G. Kolb, Th. Salbert, and G. Abstreiter in the paper "Raman-mircoprobe study of stress and crystal orientation in laser-crystallized silicon" recorded measurements from a (100)-oriented silicon wafer which was turned manually about the (100)-axis [24]. The polarization angle was varied in 5^{O} steps with constant laser power. The Raman intensity was plotted versus the polarization angle for three values of turning angle. The authors then showed that a change in crystal orientation can be resolved as a shift in the intensity of the Raman signal. The films were turned about an angle and this was observed in the Raman spectra as a shift. Therefore spectra that was shifted from the (100)-orientation plot can be used to obtain the degree of axis tilt of the film.

In the paper "Determination of local crystal orientation of diamond using polarized Raman spectra," J. Mossbrucker and T.A. Grotjohn studied the polarized Raman spectrum of a (100)-oriented diamond single crystal [25]. They developed a polar plot showing the scattered Raman intensity versus the analyzer angles for an incident polarization direction of $+45^{O}$ and -45^{O}. They plotted the experimental data versus the

theoretical values. By studying these polar plots they were able to determine the orientation of the diamond samples.

Similar techniques to these could be adapted to YBCO films for determining crystal orientation. Though these techniques may not be ideal for industrial purposes, they could still be useful in laboratory situations.

IV. Investigation of Raman Spectroscopy Experimental Setup

A. Design

The experimental setup used in this research is know as a first generation Raman spectroscopy setup, as stated in the book Modern Techniques in Raman Spectroscopy in the article "Instrumentation for Dispersive Raman Spectroscopy" by R.L. McCreary [8]. A first generation Raman spectroscopy setup consists of a double spectrometer and a photomultiplier tube. A second generation setup consists of a triple spectrometer and diode array and a third generation consists of a spectrometer and a CCD. The double spectrometer/photomultiplier tube setup is very basic and used mainly for identifying Raman lines. It allows for good resolution. The acquisition time is longer than the other two methods, but this is a necessary trade-off for this type of work.

The experimental setup is shown in Fig. 4.1. The incident electromagnetic radiation is provided by a Spectra Physics model 165 water-cooled argon ion laser. Commonly the 514 nm line was used for data acquisition. This laser emits a linear polarization parallel to the entrance slits of the spectrometer, or parallel to the z-axis in the lab frame with a polarization ratio of 100:1. The beam diameter is 1.5 mm at the 514 nm wavelength. Plasma lines are filtered out with a laser interference filter. A ½-wave plate is used to rotate the polarization vector of the laser light.

The light is then split with a beamsplitter. Half of the light then enters a lens which focuses the light onto the sample. This lens has a focal length of 28 mm and a diameter of 25 mm. This gave a spot size of 9.60 μm and a spot area of 7.85×10^{-7} cm^2. The sample is fixed onto a x-y-z translation stage. The scattered light is collected by the lens and

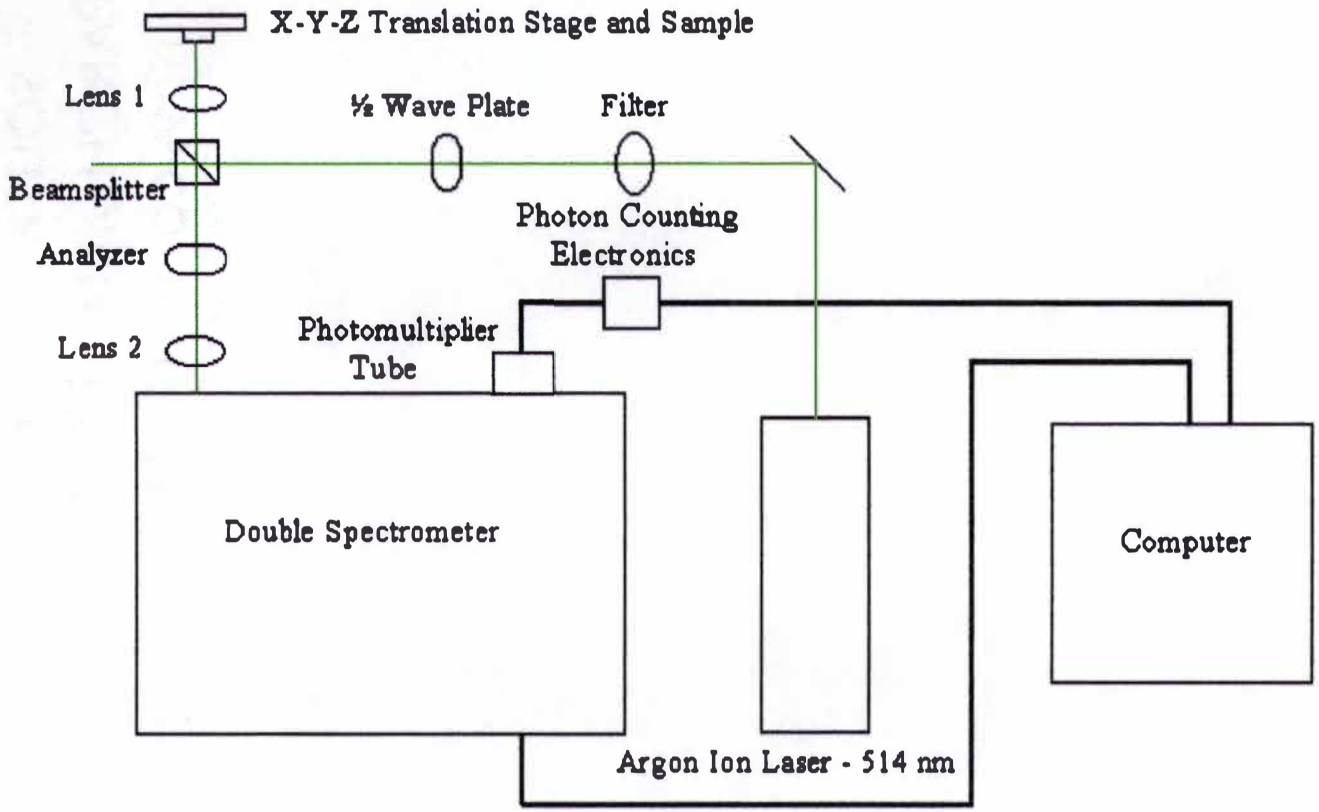


Fig. 4.1 Raman Spectroscopy Experimental Setup

passes back through the beamsplitter.

The scattered light then passes through an analyzer, allowing for selection of the scattered light polarization vector. The light is then focused onto the entrance slit of the spectrometer by a lens with a focal length of 6 cm. The spectrometer is a SPEX .85 meter double spectrometer. This spectrometer has a bandpass of 54 $\mu m/cm^{-1}$ at 514 nm, a reciprocal linear dispersion of 4.80 Angstroms/mm, and a f/# of 6. The gratings have 1200 grooves/mm.

The separated light enters a Hamamatsu R928 photomultiplier tube with a quantum efficiency of 15%, current amplification of 1×10^7, and a dark count of 25-30 counts per second. To lower shot noise, the PMT is cooled by a Products For Research, Inc. TE177RF cooler to -35° C.

The pulses are amplified using an Electron Tubes AD7 Amplifier/Discriminator and stretched using a monostable multivibrator so that the computer can detect them. The A/D has a pulse pair resolution of 24 ns and the pulse stretcher stretches each to a width of 200ns. The individual pulses are then counted by a Macintosh IIfx using a National Instruments NB-MIO-16H data acquisition card, and running LabVIEW 4.1. The LabVIEW program runs the spectrometer and counts photons. It is designed to move the spectrometer to specified spots, stop for programmed amounts of time, and count the number of photons.

B. Testing electronics

The electronics had to be tested for precision. A sodium lamp was placed in front of the entrance slit. The entrance and exit slits were opened to 20 μm. The double

spectrometer was set near an atomic line of the sodium lamp. The counter was then run for certain time intervals and the average photon counts, standard deviation, and standard deviation divided by average counts were calculated. Each time interval was run 1000 times.

Figure 4.2 is a plot of average counts versus integration time. Figure 4.3 is a plot of the log of average photon counts versus the log of integration time. The data plotted in Fig. 4.2 should fit to a line. To test if this data does fit to a line the log-log plot was used. The equation for the log-log plot shows that the data fits to a line within an error of .5%.

Figure 4.4 is a plot of the standard deviation divided by average counts verses the integration time. Figure 4.5 is a log-log plot of Fig. 4.4. The data in Fig. 4.4 should show the standard deviation/counts as a inverse square root of integration time. The log-log plot shows that the integration time has a power of -.5153 giving an error of about 2%.

These plots show that the photon counting electronics used in these experiments were precise.

C. Calibration procedures

To calibrate the setup the sodium lamp is used to align the mirrors and gratings. The emission line from the sodium lamp is peaked out according to methods described in the double spectrometer manual. The atomic line is found by scanning the spectrometer by hand. Once the line is found, the fourth mirror is adjusted to maximize the signal. Then, the spectrometer is scanned by hand again to find the peak of the line to determine the exact wavenumber for the Raman line.

The laser is then used to find the exact place for the incident radiation. The laser is

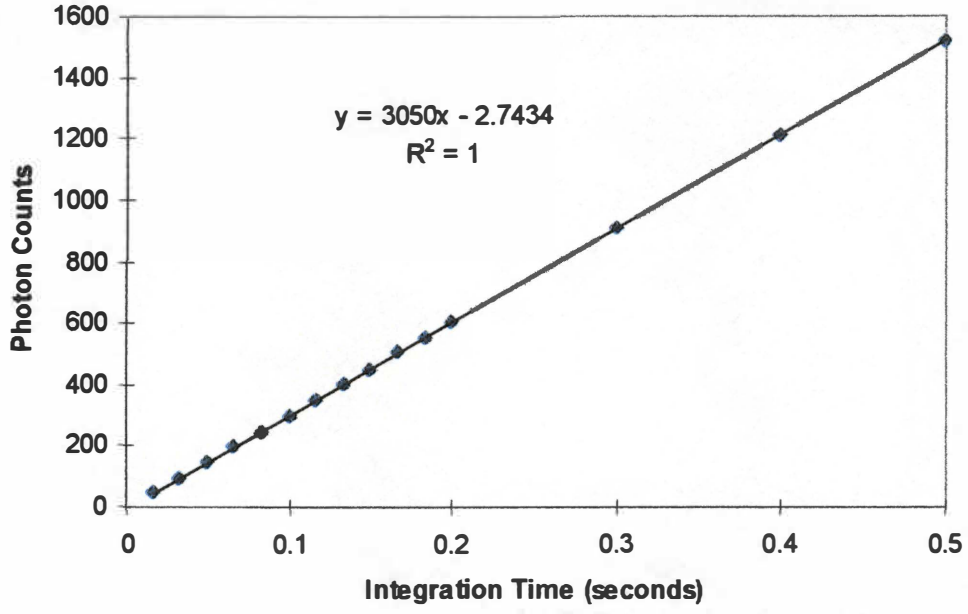


Fig. 4.2 Photon Counts vs. Integration Time

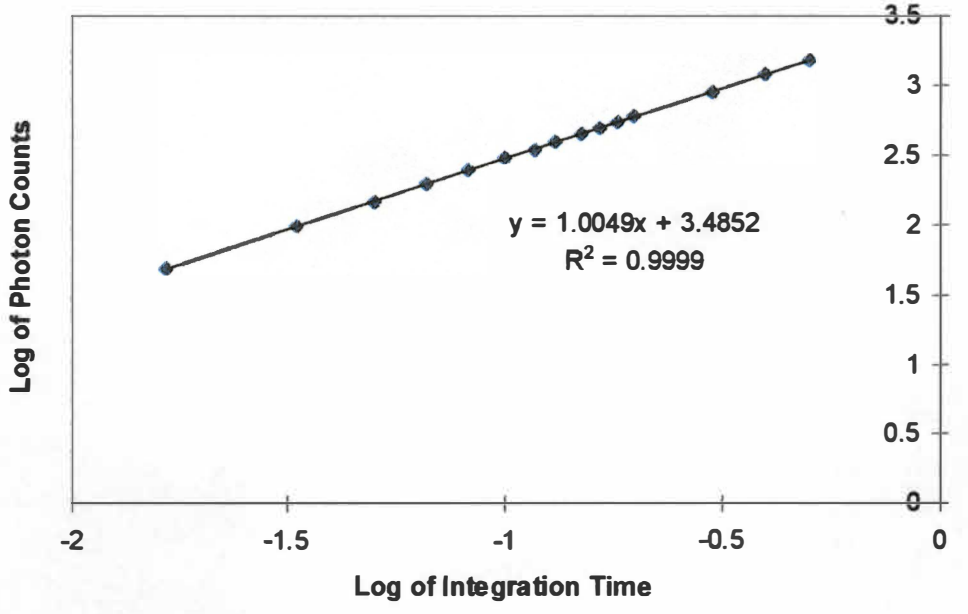


Fig. 4.3 Log of Photon Counts vs. Log of Integration Time

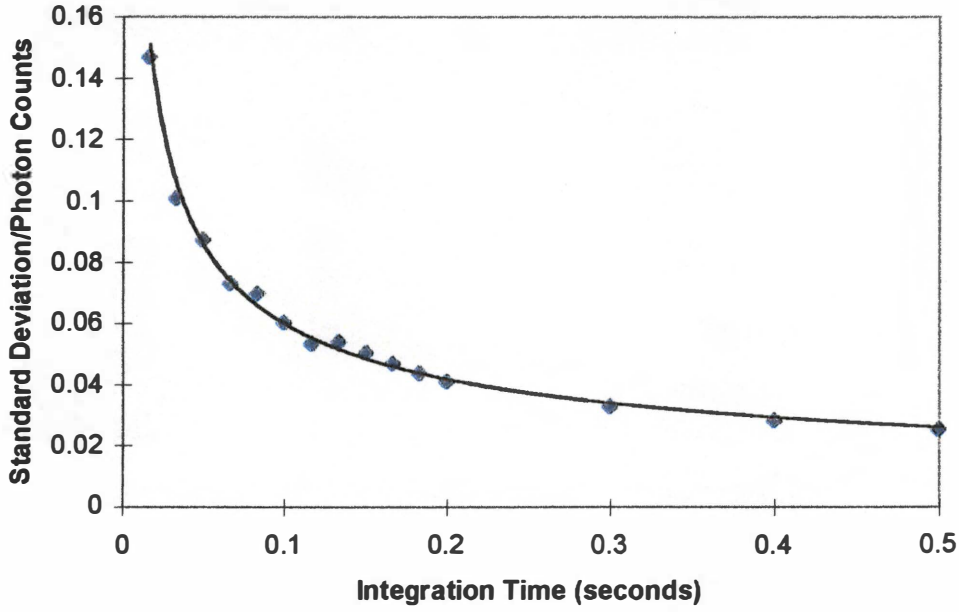


Fig. 4.4 Standard Deviation/Counts vs. Integration Time

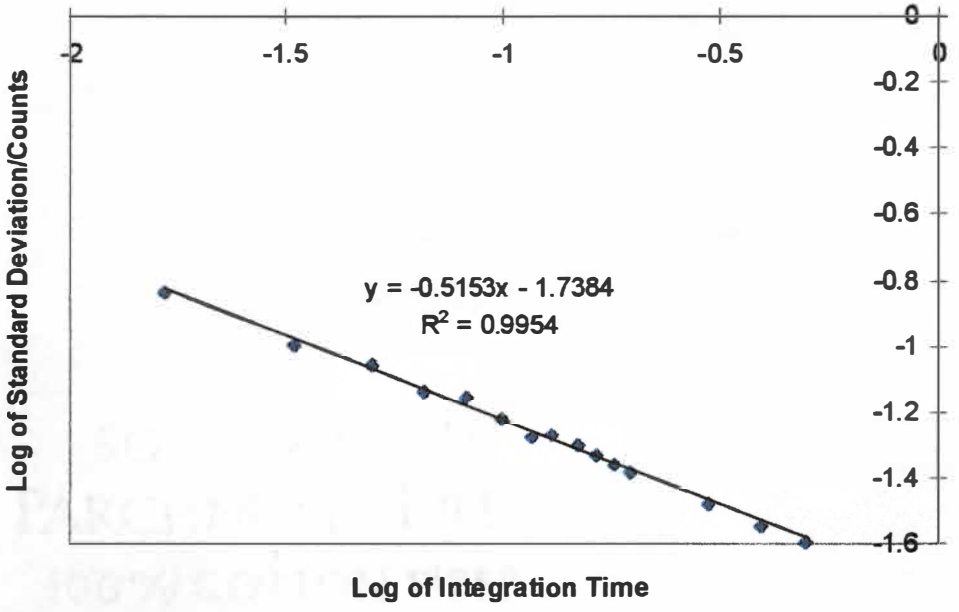


Fig. 4.5 Log of Standard Deviation/Counts vs. Log of Integration Time

used at the lowest setting and the slits are closed down to 20 microns. Once the wavenumber of the laser radiation has been determined, the setup is calibrated. This is the incident wavenumber and all wavenumber shifts are measured relative to this.

D. Data from calibration samples

To test for the accuracy of the setup, calibration samples were used. These samples were diamond and sulphur. Each of these samples have known Raman lines, and scans were performed on them to determine if the Raman spectroscopy setup performs accurate measurements.

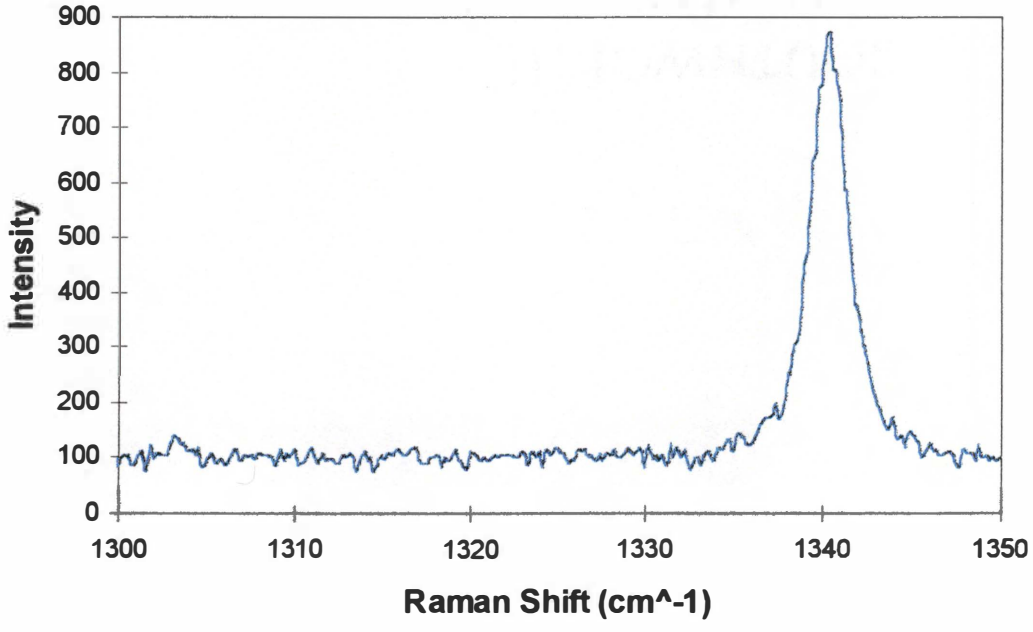


Fig. 4.6 Raman Scan on Diamond Sample

First, scans were done on a diamond sample. This scan was done with a time integration of .5 second, the slits at 20 μ -100 μ - 20 μ, and the laser at 1.5 mW. The

scan is shown in Fig. 4.6. Notice the strong Raman line at 1340 cm^{-1}. This is also the place that the Raman line was found by Mossbrucker and Grotjohn [25].

Secondly, scans were done on sulphur. Sulphur powder was used here. All of the proper Raman lines were found.

The sulphur powder was also used to investigate the effect of f/# matching. Two different scans were run on the sulphur powder. One scan was run using the described experimental setup with two lenses. A second scan was run using only one lens. The lens in front of the spectrometer was removed. This setup was used in an attempt to simplify the experimental setup. Notice in Fig. 4.7 the difference between the two scans. The scan run with the second lens in place has the higher intensity. This is due to matching the f/# of the lens to that of the spectrometer. Subsequent scans were performed using the dual lens setup.

E. YBCO film sample

The piece of YBCO film used in this thesis was scanned using several different incident polarizations and scattered polarizations. The YBCO film had a CeO_2 buffer layer and Ag/Pd/Ni substrate. The film piece had the dimensions 5 mm x 16 mm. This film should have a (001)-orientation. It was placed on the stage to correspond with the axes given in Fig. 2.1, so the c-axis of the film is parallel to the z-axis in the laboratory frame, the longer length of the film along the y-axis, parallel to the entrance slit, and the shorter width along the x-axis.

Six of the scans are included here to show the results, each corresponding to different polarization dependencies. The characteristics of all six scans were identical.

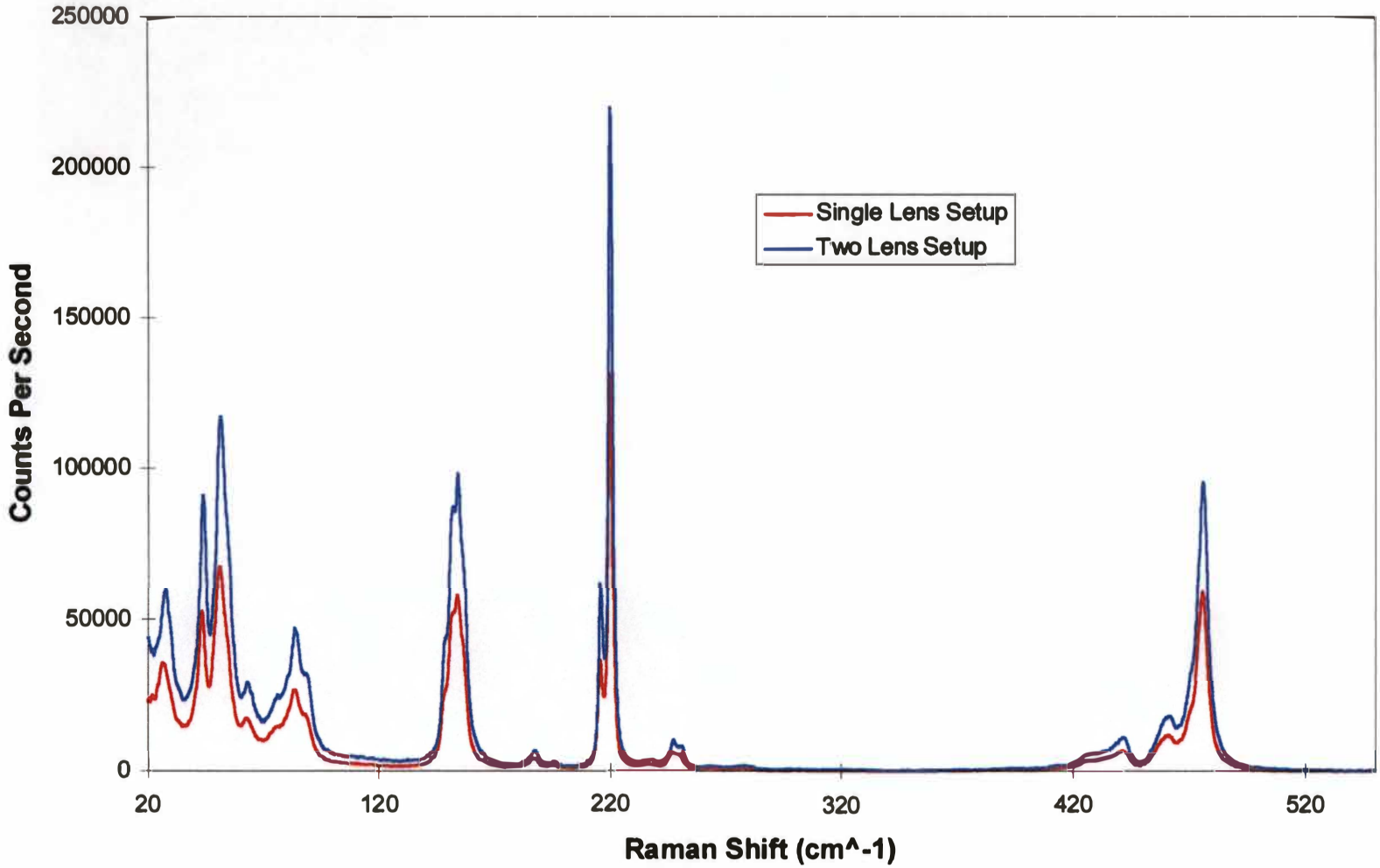


Fig. 4.7 Raman Scan of Sulphur Powder

The incident laser power was 40 mW giving a power density of 55 kW/cm^2. The photomultiplier tube voltage was 1,000 volts. The spectral bandpass was 4 cm^{-1} with the slits set at 200-200-200 μm. An integration time of 5 seconds was used.

The scan in Fig. 4.8 was taken with a yy-polarization. The scan in Fig. 4.9 was take with an incident polarization 45^O to the x-axis and scattered polarization parallel to that. Figure 4.10 shows a Raman scan which was taken with a xx-polarization. Figure 4.11 shows a scan taken with a yx-polarization. The scan in Fig. 4.12 was taken with an incident polarization 90^O to the scan in Fig. 4.9 and scattered polarization 90^O to the incident. Figure 4.13 shows a scan taken with a xy-polarization. No distinct Raman lines were obtained in these scans.

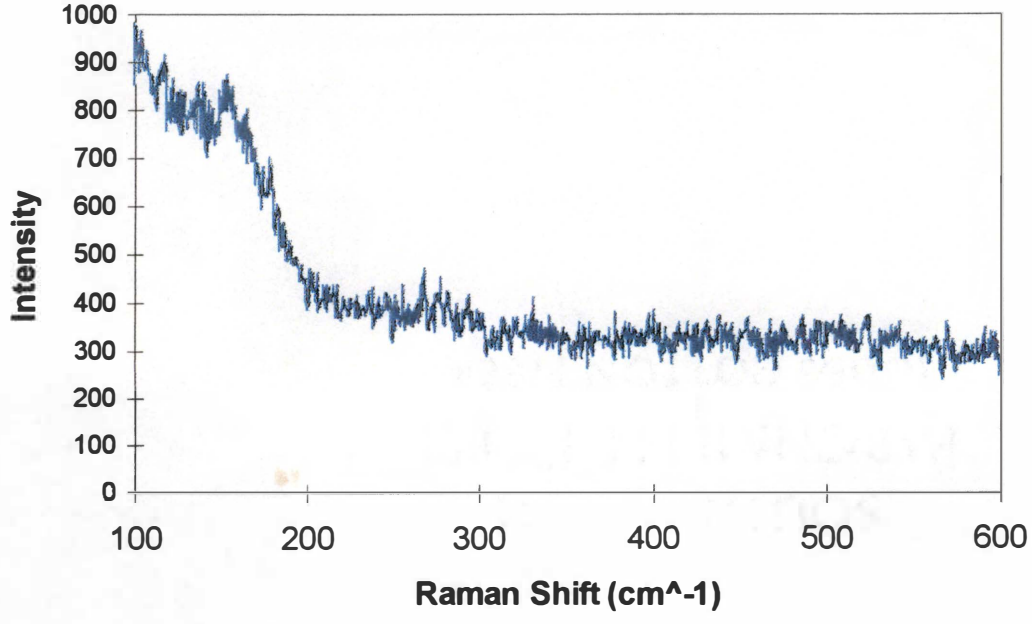


Fig. 4.8 Raman Scan on YBCO (yy-polarization)

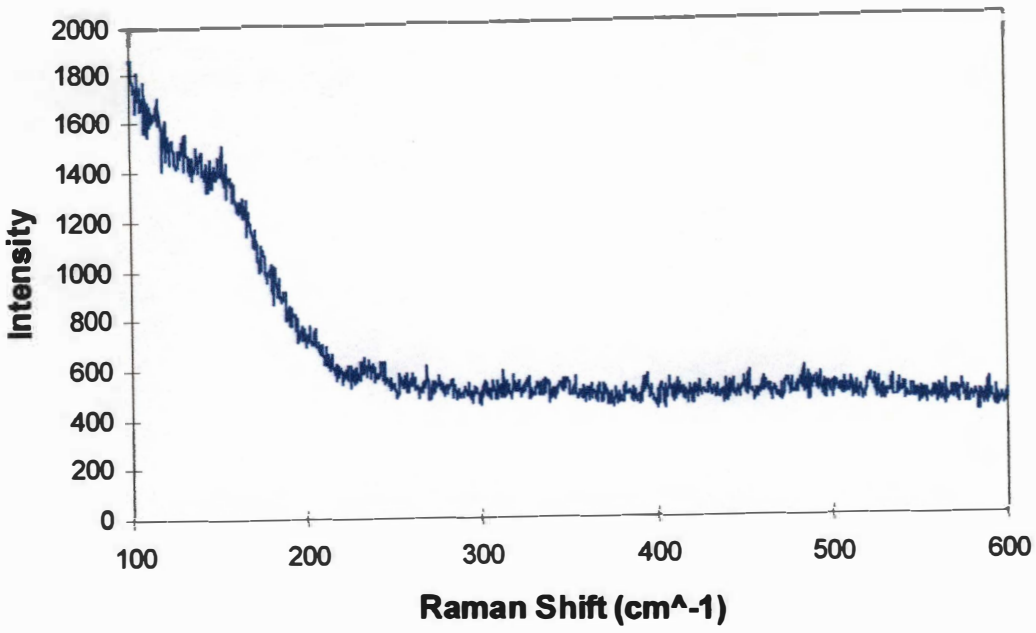


Fig. 4.9 Raman Scan on YBCO (xyxy-polarization)

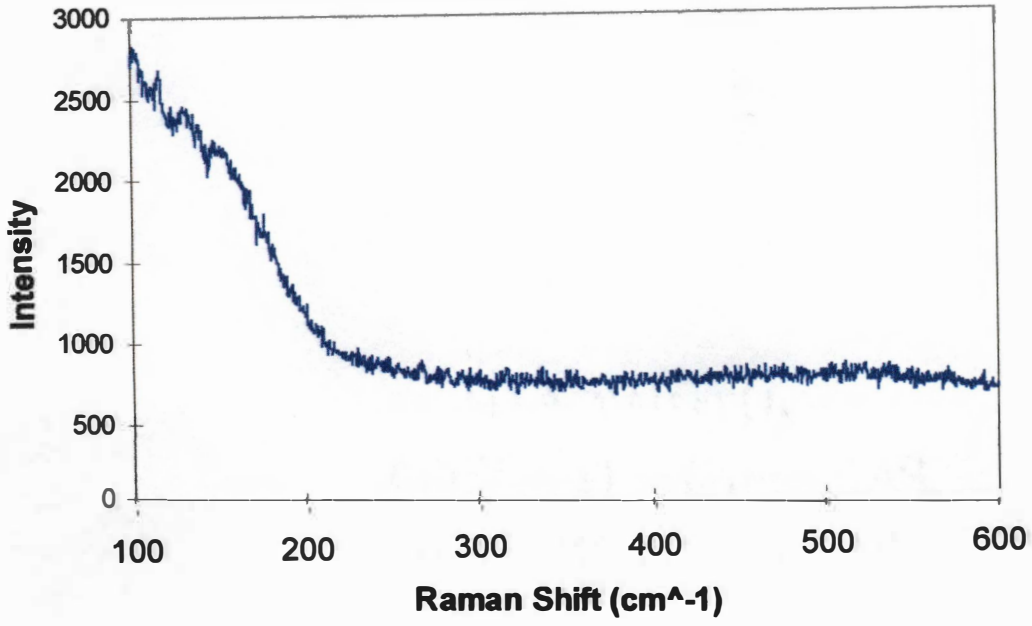


Fig. 4.10 Raman Scan on YBCO (xx-polarization)

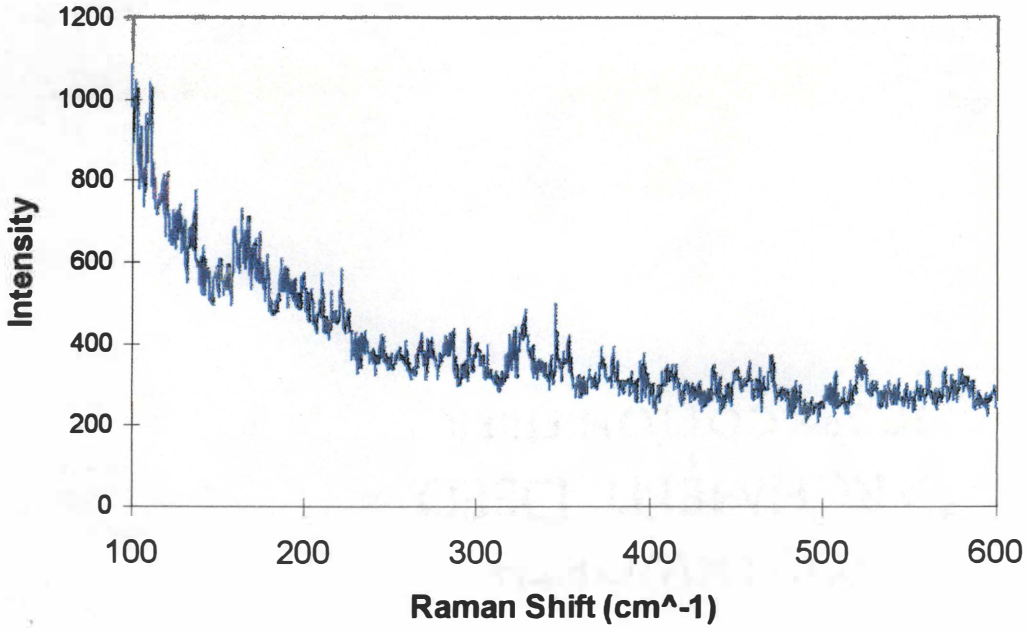


Fig. 4.11 Raman Scan on YBCO (yx-polarization)

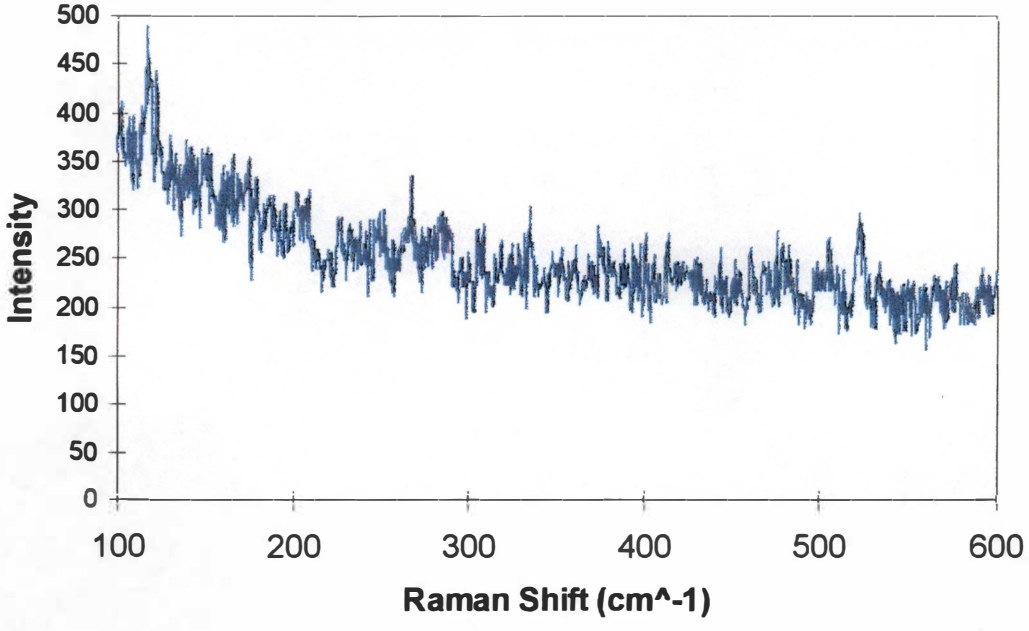


Fig. 4.12 Raman Scan on YBCO (yxxy-polarization)

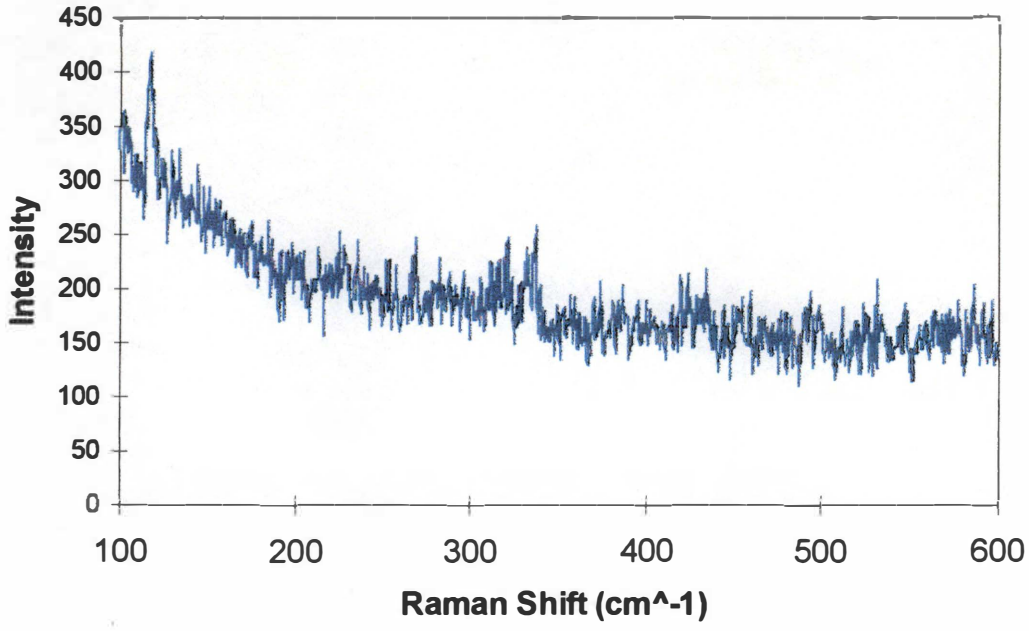


Fig. 4.13 Raman Scan on YBCO (xy-polarization)

In both scans, shown in Fig. 4.14 and 4.15, a very broad line appears at about the 335 cm^{-1} wavenumber shift. The scan in Fig. 4.14 was run with the laser power at 45 mW, giving a power density of 60 kW/cm^2, using slit widths of 220-200-220 μm, a spectral bandpass of 5 cm^{-1}, and an integration time of 10 seconds. The scan in Fig. 4.15 was run with a laser power of 35 mW, giving a power denisty of 45 kW/cm^2, using slit widths of 220-350-220 μm, a spectral bandpass of 5 cm^{-1}, and an integration time of 10 seconds. The line here is very broad. A very broad Raman spectra suggests that the film does not have a well-ordered and homogeneous crystal structure [21].

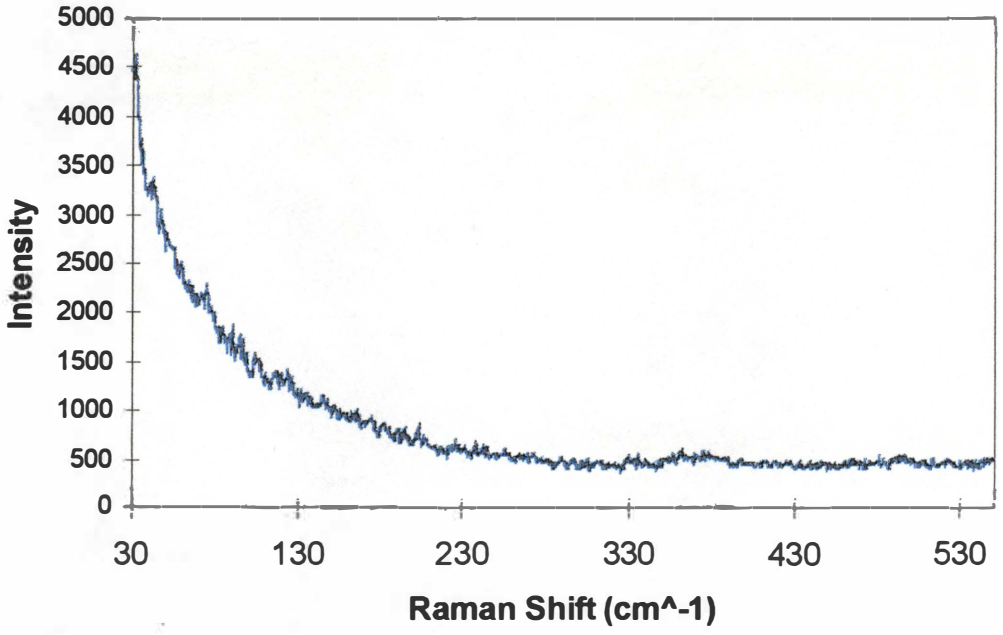


Fig. 4.14 Raman Scan on YBCO

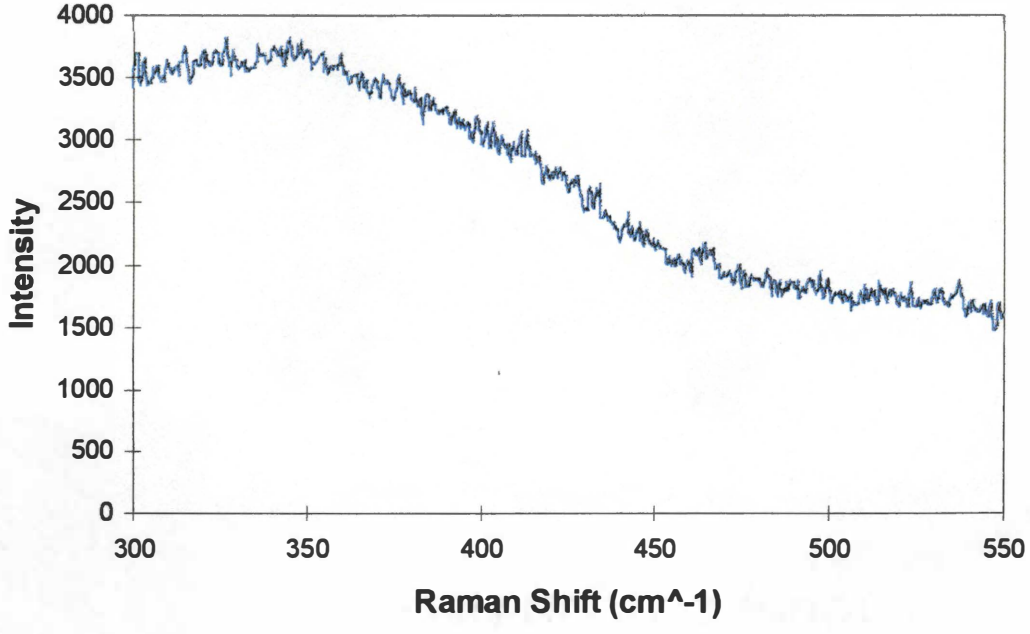


Fig. 4.15 Raman Scan on YBCO Near 335 cm^{-1} Line

F. $LaAlO_3$ sample

Raman scans were conducted on a single piece of YBCO film and a lanthanum aluminate ($LaAlO_3$) sample. Lanthanum aluminate is a material proposed as one of the buffer layers in YBCO films used specifically in the sol-gel process. This sample was provided by Vineet Lasrado, a graduate student at University of Tennessee Space Institute, who has conducted his own research on the sol-gel method for applying HTSC film layers.

Figures 4.16, 4.17, and, 4.18 show three Raman scans done on a lanthanum aluminate sample which has a strontium titanate ($SrTiO_3$) substrate. Figure 4.16 is a Raman scan taken on the middle of the film, where the layer was the thickest. There are strong Raman lines at about 330 cm^{-1} and 700 cm^{-1}. This scan was done with a laser power of 20 mW, giving a power density of 25 kW/cm^2, slit widths of 200-500-200 μm, time integration of 1 second, and spectral bandpass of 4 cm^{-1}. There was no scattered radiation polarization dependence on this scan. The scan in Fig. 4.17 was taken on the substrate itself where there was no $LaAlO_3$ layer. There is a strong line at 170 cm^{-1}. This scan had the same characteristics as the prior scan. The third figure, Fig. 4.18, was taken on an area of the film where the layer was thin. All three Raman lines can be seen, none as intense as in the prior scans. This scan was run with all of the same characteristics as the other scans.

This method can be used to obtain a qualitative measurement of layer thickness on this sample. By comparing the intensities of the Raman lines from the layer and the

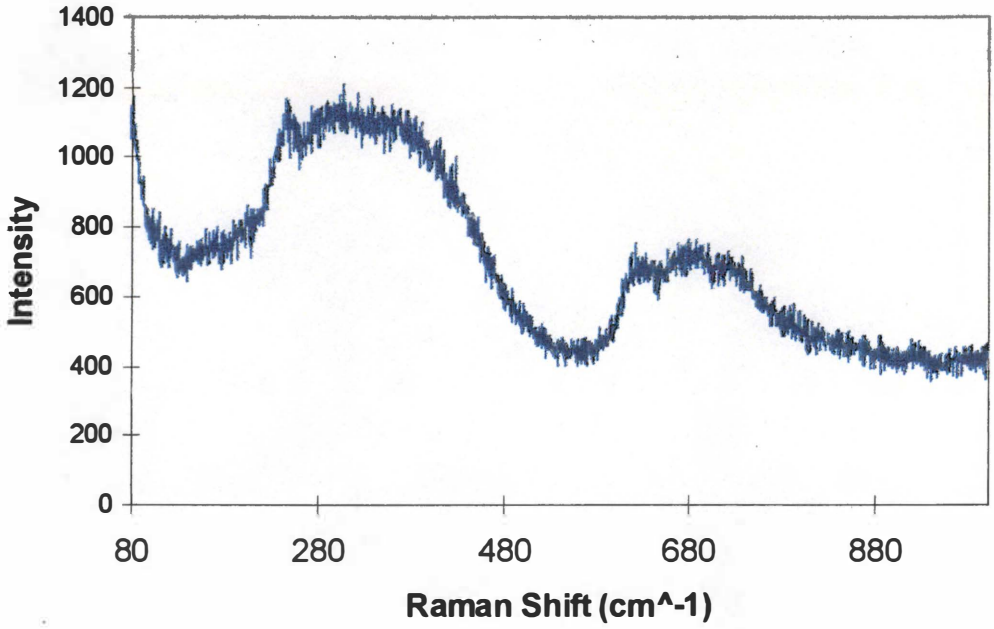


Fig. 4.16 Raman Scan on Lanthanum Aluminate Layer

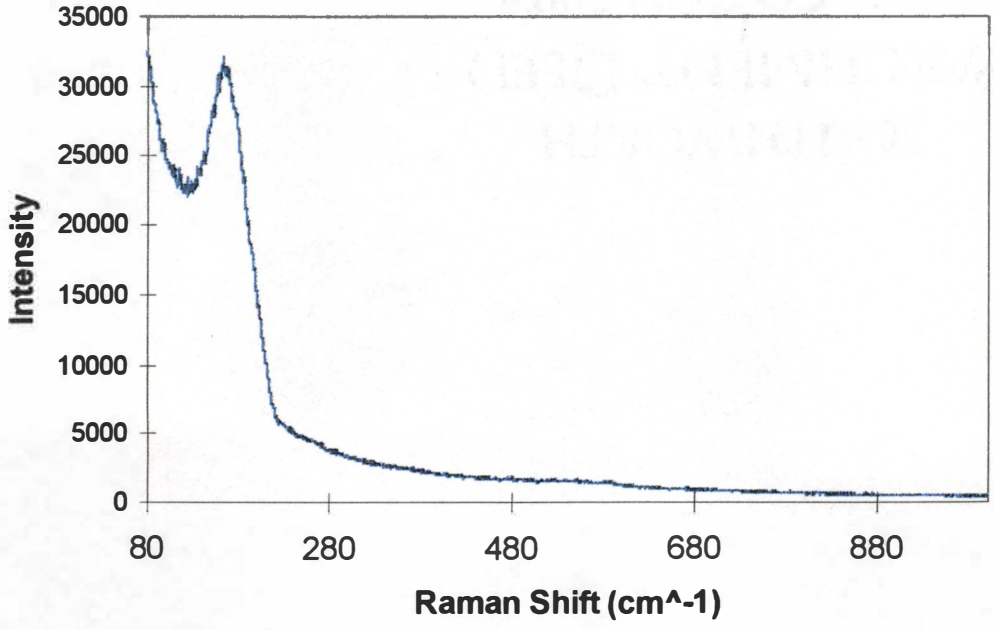


Fig. 4.17 Raman Scan on Lanthanum Aluminate Film Substrate

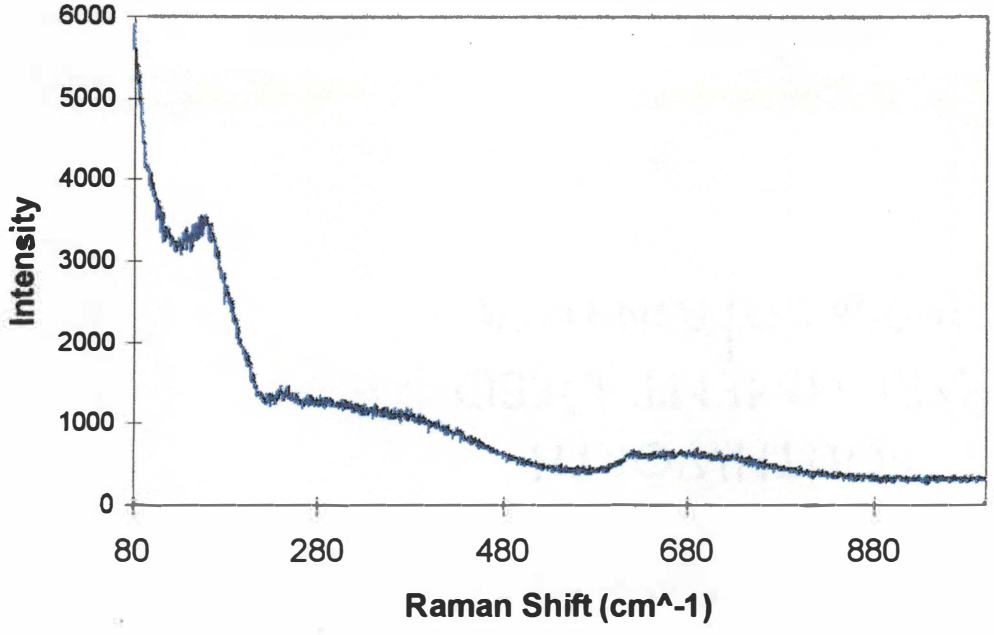


Fig. 4.18 Raman Scan on Thin Layer of Lanthanum Aluminate

substrate, the sample can be moved around in the laser beam to find areas of thicker or thinner layer thickness.

Before quantitative measurements can be made with a technique similar to the one described in this experiment calibration samples must be obtained. Samples with known layer thickness have to be used to compare layer thickness with the ratio of the Raman line from the substrate and either of the Raman lines from the layer. This would be a similar technique to that described earlier for determining YBCO layer thickness.

V. Improvements to Experimental Setup for Industrial Applications

The experimental setup in this research was used to determine the important parameters for an in situ diagnostic setup. This setup was unable to provide strong YBCO Raman lines from the film sample. The setup must be improved to provide the essential Raman line.

In this research a lens with a focal length of 28 mm was used to focus the laser light onto the film sample and the beam width was 1.5 mm giving a spot size of 9.60 μm. The spot size is calculated by multiplying the f/# with the wavelength, assuming the laser is operating in the TEM_{00} mode. The f/# is equal to the 28 mm focal length divided by the 1.5 mm beam width. This is multiplied by the 514 nm wavelength to give a spot size of 9.60 μm. Therefore, the 40 mW incident laser power gave a power density of 55 kW/cm^2. Higher power densities than this can be used without causing harm to the film. An upper parameter for power density is 150 kW/cm^2 [14, 21]. Using the same lens a laser power of 120 mW can be used without damaging the film.

The double spectrometer and photomultiplier tube arrangement appeared to have some flaws. The PM tube is supposed to have a dark count of about 3 photons/second at -35° C, but experiments showed it was only able to obtain a dark count rate of about 30 counts/second. Either the PM tube was not able to meet its specifications or the cooler was not able to cool the tube down to -35° C.

The higher dark count rates provided by this PM tube, along with background noise, could be hiding the Raman signal. In figures showing crossed polarizations the count rates approach a level of about 30 counts/second, suggesting the signal is purely the dark signal. Count rates of Raman lines from YBCO are rather small [20]. Raman lines in

parallel polarizations have count rates of 250-150 counts/second. Raman lines in crossed polarizations have count rates of 100-50 counts/second. In the Raman scans run in this research, background signals varied from 60 to 200 counts/second in parallel polarizations. Raman scans run with crossed polarizations had background signals of 30 to 100 counts/second. These background signals could definitely hide any Raman signals.

Future experimental setups should be designed to increase the signal. One method of doing this is by increasing the number of Raman scattered photons. The number of particles scattered per second is given by

$$\frac{\#scattered}{\sec} = \frac{\#incident / \sec}{A}\eta\sigma, \tag{15}$$

where A is the sample area, σ is the total Raman cross section, and η is the number of scatterers. The number of scatterers is given by

$$\eta = nLA, \tag{16}$$

where L is the probe length into the sample and n is the density of scatterers. Therefore equation (15) becomes

$$\frac{\#scattered}{\sec} = \frac{\#incident}{\sec}nL\sigma. \tag{17}$$

The variables n, L, and σ will all be constant for YBCO film samples. Therefore to increase the number of scattering photons the number of incident photons must be increased. The number of incident photons is given by

$$\frac{P}{h\nu} = \frac{P}{hc}\lambda = \frac{EA}{hc}\lambda, \tag{18}$$

where P is the incident laser power, hν is the energy per photon, and E is the incident laser power density (laser power divided by the sample area). The highest possible value for E

has been determined to be 150 kW/cm^2. Therefore the sample probe area can be increased, but the incident laser power must be increased to keep the power density constant. Also higher wavelengths could be used.

The signal from Raman scattering is given by

$$S = E\frac{d\sigma}{d\Omega}nA\Omega TQKNt \tag{19}$$

where $\frac{d\sigma}{d\Omega}$ is the scattering cross section, Ω is the collection angle, T is the transmission of the optics and spectrometer, Q is the quantum efficiency, K is a geometric factor which accounts for the probability that the scattered light will pass through the input aperture, N is the number of channels monitored, and t is the integration time [8]. For a PM tube setup N would be 1.

There are a number of ways to increase signal. A maximum power density of 150 kW/cm^2 can be used. The scattering cross section and the number density of crystals are constant for YBCO, therefore only the other variables can be altered. For an industrial in situ process the integration time t will be limited to the order of a second. The transmission of the optics, collection angle, and number of channels can all be increased to increase signal. The collection angle is equal to the probed sample area divided by the focal length of the lens squared. Increasing the collection angle will increase the detected signal from any given crystal , but the area will decrease. Using a lens with a smaller f/# will increase the collection angle.

The problem then becomes to match the f/# of the lens at the sample to the f/# of the spectrometer to maximize throughput. The lens in front of the spectrometer should have an f/# equal to that of the spectrometer. A diverging lens placed after the sample

lens and before the focal point will give the diameter needed at the spectrometer lens and provide a collimated beam to the spectrometer.

The signal intensity is limited by the noise. The signal to noise ratio is the ratio of the true signal intensity divided by the r.m.s. fluctuations of the signal from its true value. The noise can be classified as either shot noise or flicker noise. Shot noise arises from the quantum nature of matter and photons. The shot noise component of any noise is equal to the square root of the magnitude of that component and can only be reduced by reducing the magnitude of the component which produces it. Flicker noise is directly proportional to the magnitude of the signal and cannot be reduced without reducing the signal which produces it [8].

Improvements in signal to noise ratio can be achieved by reducing the background noise which is composed of the dark count and the blank noise. Blank noise arises from the Raman and Rayleigh scatter. Multiple stage instruments are commonly used to reject the scatter. Cut-off interference filters or holographic notch filters can be used to reduce laser scatter. The maximum signal to noise ratio is possible at a given signal level where the noise is due entirely to shot noise on the signal [8].

One method of increasing signal is to use multichannel detectors. Using a multichannel detector with N channels can increase signal to noise ratio by a square root of N over the ratio obtained using a single channel or PM tube in the same amount of time.

Future research should involve an experimental setup utilizing these various improvements. The use of multichannel detectors can increase signal to noise ratio. Efforts to increase signal using a higher power density and a larger collection angle will

increase the signal. Signal to noise ratio can also be increased by using detectors with lower dark counts and a higher quantum efficiency than those used in this thesis.

VI. Conclusion

The need for in situ diagnostics in the manufacture of HTSC films can be met with a Raman spectroscopy technique. Previous work concerning YBCO films documents the large amount of information that can be obtained using Raman spectroscopy. Information on oxygen concentration, crystal orientation, and layer thickness can be determined.

Raman spectroscopy not only supplies information about the YBCO layer, but also about any of the buffer layers or the substrate. Techniques similar to those used for the YBCO layer could also be used for any of these other layers. This thesis presents a method for determining layer thickness of YBCO layers. This method could be adapted to determine the thickness of buffer layers, such as $LaAlO_3$.

The Raman spectroscopy techniques, as described in this thesis, would have to be adapted to acquire the needed data for in situ diagnostics. Such a technique could use a laser diode to irradiate the film. The light could be detected by two photodiodes, each utilizing filters to pick out certain Raman lines. For example, by detecting the 500 and 335 cm^{-1} lines the degree of c-axis tilt of the YBCO film could be found. Such a technique could also be used to determine layer thickness in any of the other layers by using the proper Raman lines.

More research and improvements to the experimental setup must be done before specific industrial applications are determined. The setup must be adapted to acquire data within the time constraints of an industrial setting. By using the methods outlined in this thesis, for increasing Raman signals and signal to noise ratios, a Raman technique should be able to be designed for online, real time data acquisition. Raman spectroscopy research

shows promise as a possible diagnostic technique for the in situ monitoring of film layer quality.

References

References

1. Sheahen, Thomas P., Introduction to High-Temperature Superconductivity, Plenum Press, New York, 1994.

2. Goyal, A. et. al., "High Critical Current Density Superconducting Tapes By Epitaxial Deposition of YBCO Thick Films on Biaxially Textured Metals," Applied Physics Letters, Sep. 19, 1996.

3. DOE Topical Report "Evaluation of Methods for Application of Epitaxial Layers of Superconductor and Buffer Layers." June 1997, work performed under contract No. DE-AC-2295PC95231. Prepared by University of Tennessee Space Institute.

4. Dieckmann, N., Bock, A., Merkt, U., "Spatially resolved analyses of epitaxial and electrical properties of $YBa_2Cu_3O_7$ devices," Applied Physics Letters, Vol. 68, No. 25, June 17, 1996.

5. Bock, A., Kursten, R., Bruhl, M., Dieckmann, N., Merkt, U., "Desorption of oxygen from $YBa_2Cu_3O_{6+x}$ films studied by Raman spectroscopy," Physical Review B, Vol. 54, No. 6, August 1, 1996.

6. Garcia-Gonzalez, E., et. al., "Microstructural analysis of $YBa_2Cu_3O_y$ thin films deposited on $SrTiO_3$ and $LaAlO_3$ substrates by off-axis magnetron sputtering," Journal of Applied Physics, Vol. 78, No. 1, July 1, 1995.

7. Thomsen, C., et. al., "Systematic Raman and Infrared Studies of the Superconductor $YBa_2Cu_3O_{7-x}$ as a Function of Oxygen Concentration," Solid State Communications, Vol. 65, No. 1, 1988.

8. Laserna, J.J., Modern Techniques in Raman Spectroscopy, John Wiley & Sons Ltd., Chichester, 1996.

9. Faulques, Eric and Russo, Richard E., "Characterization of High Temperature Superconductors with Rāman Spectroscopy," Applications of Analytical Techniques to the Characterization of Materials, ed. Perry, Plenum Press, New York, 1991.

10. Faulques, Eric, "Raman Spectra of Unconventional Superconductors," to appear in Synthesis of Materials Characterization, ed. Perry, Plenum Press, New York.

11. Hopkins, J.B., Farrow, L.A. "Raman microprobe determination of local crystal orientation," Journal of Applied Physics, Vol. 59, No. 4, February 15, 1986.

12. Ashcroft, Neil W., Mermin, N. David. Solid State Physics. Holt, Rinehart, and Winston, New York, 1976.

13. Zetterer, T. et. al., "Preparation, characterization, and far-infrared study of ceramic high-T_c superconductors," Journal of Optical Society of America B, Vol. 6, No. 3, March 1989.

14. Gasparov, L.V., "Phonon-mode characterization of orthorhombic and tetragonal $YBa_2Cu_3O_{7-\delta}$ single crystals by Raman spectroscopy," Journal of Optical Society of America B, Vol. 6, No. 3, March 1989.

15. Hemley, R.J., Mao, H.K., "Single crystal micro-Raman spectroscopy of phases in the Y-Ba-Cu-O superconductors," Physical Review Letters, Vol. 58, No. 22, June 1, 1987.

16. McCarty, K.F., "Raman-active phonons of a twin-free $YBa_2Cu_3O_7$ crystal : A complete polarization analysis," Physical Review B, Vol. 41, No. 13, May 1, 1990.

17. Aleksandrov, I.V. et. al., "Raman scattering in single crystals of $YBa_2Cu_3O_x$ high-temperature superconductors," JETP Letters, Vol. 47, No. 4, February, 25, 1988.

18. Hangyo, M., et. al., "Effect of Oxygen Content on Phonon Raman Spectra of $YBa_2Cu_3O_{7-\delta}$," Solid State Communications, Vol. 65, No. 8, 1988.

19. Krol, D.M., et. al., "Raman spectroscopy of single crystals of high-Tc cuprates," Journal of Optical Society of America B, Vol. 6, No. 3, March 1989.

20. Karmanenko, S.F., et. al., "Influence of the growth rate of $YBa_2Cu_3O_{7-\delta}$ films on the orientation of the crystallographic axes," Technical Physics Letters, Vol. 22, No. 12, December 1996.

21. Jahanzeb, A., Celik-Butler, Z., Shan, P.C., Butler, D.P., "Studies and implications of the Hall effect in superconducting and semiconducting $YBa_2Cu_3O_{7-\delta}$ thin films," Journal of Applied Physics, Vol. 78, No. 11, December 1, 1995.

22. Belousov, M.V., et. al., "Raman scattering of light used as a method of analyzing the oriented $YBa_2Cu_3O_{7-\delta}$ films," JETP Letters, Vol. 48, No. 5, September 1988.

23. Zhang, P., Haage, T., Habermeier, H.-U., Ruf, T., Cardona, M., "Raman spectra of ultrathin $YBaCuO_{7-\delta}$ films," Journal of Applied Physics, Vol. 80, No. 5, September 1, 1996.

24. Kolb, R., Salbert, Th., Abstreiter, G., "Raman-microprobe study of stress and crystal orientation in laser-crystallized silicon," Journal of Applied Physics, Vol. 69, No. 5, March 1, 1991.

25. Mossbrucker, J., Grotjohn, T.A., "Determination of local crystal orientation of diamond using polarized Raman spectra," Diamond and Related Materials, Vol. 5, 1996.

26. Farrow, L.A., Hopkins, J.B., Fisanick, G.J., "Local crystal orientation in laser annealed silicon using a Raman microprobe," Material Resources Society Symposium Proceedings, Vol. 29, 1984.

27. Mizoguchi, Kohji, and Nakashima, Shin-ichi, "Determination of crystallographic orientations in silicon films by Raman-microprobe polarization measurements," Journal of Applied Physics, Vol. 65, No. 7, April 1, 1989.

28. Lee, Y.H. et. al., "Vapor deposition of diamond thin films on various substrates," Applied Physics Letters, Vol. 57, No. 18, October 29, 1990.

Vita

Jason Cunningham was born in Frederick, Maryland on July 6, 1974. He lived there for fifteen years before moving to Augusta, Georgia, where he graduated from Lakeside High School in 1992. Then, he attended Berry College in Mt. Berry, Georgia. He graduated with Bachelor's Degrees in Physics and Mathematics in 1996. He then moved to Tullahoma, Tennessee to begin his graduate work at the University of Tennessee Space Institute. On May 24, 1997 he married Heather Paige Whitfield. In 1998 he received his Master's Degree in Physics.

Currently he and his wife reside in Dublin, Ohio. Jason is working as a Diagnostics Engineer at Diamond Power Specialty Company in Lancaster, Ohio.

5264 1472 20
08-04-99 MAB
INFORMATION CONSERVATION, INC.